2016

Quantitative Functional Magnetic Resonance Imaging of Multiple Sclerosis

Bird, Jaimie

UNIVERSITY OF CALGARY

Quantitative Functional Magnetic Resonance Imaging of Multiple Sclerosis

by

Jaimie Bird

A THESIS

SUBMITTED TO THE FACULTY OF GRADUATE STUDIES

IN PARTIAL FULFILMENT OF THE REQUIREMENTS FOR THE

DEGREE OF MASTER OF SCIENCE

GRADUATE PROGRAM IN MEDICAL SCIENCE

CALGARY, ALBERTA

JUNE, 2016

Abstract

Magnetic resonance imaging (MRI) and functional MRI (fMRI) continue to advance the understanding of multiple sclerosis (MS) pathology, but these conventional imaging techniques have several limitations, which may render them insufficient to identify biomarkers of a disease as multifaceted as MS. This thesis employed quantitative fMRI to investigate uncharted measures of MS cerebral physiology, which can contribute to the development of new MS biomarkers; specifically, motor cortex flow-metabolism coupling and global grey matter cerebrovascular reactivity (CVR) were quantified. Data analysis of 12 MS patients and 11 healthy controls revealed between-group differences in cerebral blood flow (CBF) and oxygen metabolism. However, the ratio between CBF and oxygen metabolism, as well as CVR, had no significant between-group differences. These findings provide preliminary information about MS pathology and potential MS biomarkers. This research also demonstrates limitations of quantitative fMRI that impede the ability to make robust conclusions; therefore, further methodological research is needed.

Acknowledgements

First and foremost I would like to thank my supervisor, Dr. Bruce Pike, for providing me with an amazing research experience and expanding my passion for research. Your support and mentorship over the past two years has meant more than you know. I could not have asked for a better supervisor.

Thank you to my committee members, Dr. Andrea Protzner and Dr. Marcus Koch, for your thoughtful feedback and guidance. Thank you Dr. Jeff Dunn, for being on my thesis examining committee.

I am extremely grateful for all of my lab members for creating a friendly and collaborative environment. Specifically, I would like to thank Kristin Sabourin for helping with data collection. Additionally, special thanks to Dr. Erin Mazerolle for helping me every step of the way; I don't know what I would have done without you!

Many thanks to Dr. Randall Stafford for your continuous support and for sharing your MR physics expertise.

I would also like to acknowledge the Seamen Family MR Research Centre and my funding resources, specifically the NSERC I3T scholarship and the Queen Elizabeth II scholarship.

Thank you to all of the study participants; none of this would have been possible without you.

And of course, thank you to my friends and family, and especially to Sam, for supporting me and for helping me maintain a good work-life balance.

This thesis is dedicated to Dr. Bruce Pike's research team and the research participants.

Table of Contents

List of Tables

List of Figures

List of Abbreviations

ΔBOLD	BOLD percent signal change during activation
ΔCBF	CBF percent signal change during activation
$\Delta CBF/\Delta CMRO_2$	Flow metabolism ratio
$\Delta CMRO_2$	$CMRO_2$ percent signal change during activation
9-HPT	9-hole peg test
ASL	Arterial spin labeling
ASSET	Array coil Spatial Sensitivity Encoding
ATP	Adenosine triphosphate
B_0	Main magnetic field along the z-direction
BBR	Boundary based registration
BET	Brain extraction tool
BOLD	Blood-oxygen-level-dependent
CBF	Cerebral blood flow
CBV	Cerebral blood volume
$CMRO_2$	Cerebral metabolic rate of oxygen
CNS	Central nervous system
CVR	Cerebrovascular reactivity
DOF	Degrees of freedom
EAE	Experimental autoimmune encephalomyelitis
EDSS	Expanded disability status scale
EPI	Echo-planar imaging
$ETCO_2$	Partial pressure of end-tidal carbon dioxide
FAST	FMRIB's automated segmentation tool
FLAIR	Fluid-attenuated inversion recovery
FLAME	FMRIB's local analysis of mixed effects
FLIRT	FMRIB's linear registration tool
fMRI	Functional magnetic resonance imaging
FSL	FMRIB software library
FWHM	Full-width half-maximum
GM	Gray matter
GRE	Gradient recalled echo
GWAS	Genome-wide association study
HC	Healthy control
ME	Motor execution
MFIS	Modified fatigue impact scale
MHI	Mental health inventory
MI	Motor imagery
mm Hg	Millimeters of mercury
MNI	Montreal neurological institute
MR	Magnetic resonance
MRI	Magnetic resonance imaging
MS	Multiple sclerosis
NAWM	Normal appearing white matter
NMV	Net magnetization vector

OEF	Oxygen extraction fraction
pCASL	Pseudo-continuous arterial spin labeling
PPMS	Primary progressive multiple sclerosis
psc	Percent signal change
PURE	Phased array uniformity enhancement
RF	Radio frequency
RNS	Reactive nitrogen species
ROI	Region of interest
ROS	Reactive oxygen species
RRMS	Relapsing remitting multiple sclerosis
SD	Standard deviation
SDMT	Symbol digit modality test
SE	Spin echo
SNR	Signal-to-noise ratio
SPM	Statistical parametric mapping
SPMS	Secondary progressive multiple sclerosis
SPSS	Statistical package for the social sciences
T-25FW	Timed 25 foot walk
T_1	Spin-lattice relaxation time constant
T_2	Spin-spin relaxation time constant
T_2*	Effective reduced spin-spin relaxation constant
TCD	Transcranial Doppler
TE	Echo time
TR	Repetition time
tSNR	Temporal signal-to-noise ratio
WM	White matter

Chapter One: Introduction

Multiple sclerosis (MS) is a demyelinating autoimmune disease of the central nervous system that can produce neurological symptoms ranging from motor deficits and cognitive decline to psychiatric problems. These symptoms can have a complex and variable time course due to acute focal tissue damage and repair, functional reorganization of the brain, and underlying progressive pathology. While considerable progress has been achieved in the development of therapies that suppress acute focal attacks, neuroplasticity and disease progression in MS are poorly understood.

Since its development in the 1970s, magnetic resonance imaging (MRI) has been used to investigate the underlying pathology of numerous diseases, including MS. Currently the primary application of MRI in MS patients is its ability to localize MS lesions. Unfortunately, the occurrence of these lesions does not always correlate strongly with the clinical presentation of the disease, so this structural information is limited in its ability to explain or predict MS progression. Functional MRI (fMRI) is now a commonly used research tool that provides information about brain function, and could complement the information provided by structural MRI.

fMRI research is attempting to provide a more comprehensive explanation of MS pathology and progression. Thus far, fMRI MS studies have identified a number of cerebral physiological processes that appear to be abnormal in MS [1-3]; however, it is challenging to make sense of the literature due to inconsistency of results. These inconsistencies suggest that some undefined, unaccounted for, pathological process might be affecting the data, and conventional fMRI techniques may therefore be insufficient to accurately assess and explain MS pathophysiology.

Conventional blood-oxygen-level-dependent (BOLD) fMRI is limited by its qualitative nature and its reliance upon a fixed relation between blood flow and oxygen metabolism responses to neural activity. This fixed flow-metabolism coupling has been characterized in healthy people, but it has been suggested to be abnormal in MS. The ability of BOLD fMRI to reliably assess functional reorganization in MS is therefore uncertain. New fMRI techniques can provide quantitative measures of cerebral physiology, including assessing flow-metabolism coupling, as well as cerebral vascular reactivity (CVR). Flow-metabolism coupling is the coordinated spatial and temporal response that follows an increase in neural activity, whereby the vascular system increases blood flow to the activated cortical area to meet the increased energetic demands. CVR is an indicator of the ability of cerebral arterioles and capillaries to increase blood flow during neural activation. In addition to helping characterize the BOLD response in MS patients, quantification of these measures offers information about potential new biomarkers of MS cortical pathology and/or disease progression.

This thesis aimed to advance the understanding of MS pathology by using quantitative fMRI techniques to investigate measures of cerebral physiology in MS patients compared to healthy controls. Specifically, I had two primary research objectives:

1) To investigate whether the flow-metabolism relationship, as well as BOLD, cerebral blood flow (CBF), and cerebral metabolic rate of oxygen ($CMRO_2$) percent signal change (psc), are altered in the motor cortex of relapsing remitting MS (RRMS) patients versus healthy controls,

   and

2) To determine if gray matter cerebrovascular reactivity is impaired in these same RRMS patients.

As an extension of objective 1, we also analyzed whether a motor imagery (MI) task can successfully activate the motor cortex in MS patients, in order to assess motor cortical activation independent of physical hand function. MI has been shown to activate similar regions as motor execution (ME) in healthy controls [4], but this has never been studied in MS patients.

The primary objectives of this research are important to determine the validity of BOLD fMRI for the assessment of functional reorganization in MS patients, and to explore new potential markers of MS pathophysiology that may provide a window on the progressive component of the disease and/or cortical pathology.

This thesis consists of six chapters. This chapter, Chapter 1, provided a brief introduction outlining the motivation and primary objectives of this research. Chapter 2 provides a more extensive background on the primary topics discussed in this thesis, including sections on multiple sclerosis, basic principles of MRI, and fMRI, which summarizes the relevant existing fMRI research on MS. Chapter 3 describes the methodology used in this thesis, and is comprised of four sections: a description of the study population, the experimental design, the study protocol, and the data analysis pipeline. Chapter 4 includes the results of the two main research objectives. Chapter 5 provides a discussion of the results and how these findings fit in with the previous literature. The last chapter, Chapter 6, gives an overall conclusion, as well as limitations and future directions of the presented research.

Chapter Two: Background

2.1 Multiple Sclerosis

2.1.1 Disease characteristics, symptoms, and epidemiology

MS is a chronic disease of the central nervous system (CNS), affecting the brain, spinal cord, and optic nerves. It is characterized by inflammation and demyelination caused by a maladaptive autoimmune response. MS is the most common chronic neurological disease affecting young adults in Canada, with a peak age of onset at about 30 years [5, 6], and is two to three times more common in females than males [6-9]. Canada has the highest reported incidence rate of MS in the world, with the current patient population estimated to be as high as 100,000 [5].

MS is an extremely heterogeneous disease, often presenting differently in different patients. Common symptoms of MS include blurred vision, poor bladder control, burning or stabbing pains, difficulties thinking, and coordination/balance deficits [10-12]. Eighty percent of patients will report severe physical and cognitive fatigue [13-15]. MS patients also appear to have a higher prevalence of psychiatric symptoms compared to the general population, including above-average symptoms of depression and anxiety [16, 17]. Additionally, almost all MS patients experience motor symptoms, including trouble walking, muscle weakness or spasms, numbness, and impaired fine motor movements [11, 18, 19].

2.1.2 Pathophysiology

MS was first described by Charcot in 1868, and it has since been characterized by recurrent attacks of focal demyelination (lesions) in the white matter (WM) of the brain and

spinal cord [20-22]. The exact cause of MS is unknown; however, it is thought to involve a multitude of factors, including genetic, environmental, and immunological.

The occurrence of MS lesions is directly associated with the immune system and the inflammatory response. The cause of this inflammation involves an autoimmune response of irregular immune cells attacking myelin self-antigens in the CNS [23-25]. This autoimmune response is most likely triggered by the activation of myelin-specific T-cells, which are more frequently activated in MS patients compared to healthy controls [25]. These autoreactive T-cells, specifically CD4+ helper-T cells, are able to penetrate the blood brain barrier, where they recognize myelin antigens as being foreign and therefore initiate an inflammatory response in the CNS [26]. The surrounding myelin is then destroyed by macrophages, resident microglia, astrocytes, and cytokines. This immunological process is similar to the underlying process that occurs in experimental autoimmune encephalomyelitis (EAE), which is an inflammatory demyelinating disease of the CNS and is commonly used as an animal model of MS [26, 27].

In addition to this pathological autoimmune component, progressive neurodegeneration is also seen in the majority of MS cases. The previously discussed chronic inflammation causes production of reactive oxygen and nitrogen species (ROS and RNS, respectively); these free radicals interfere with mitochondrial DNA synthesis, resulting in mitochondrial injury and therefore metabolic stress [28, 29]. Insufficient energy supply results in neurodegeneration of neurons and oligodendrocytes. This neurodegeneration causes disability and is associated with progressive worsening of the disease [29].

Beyond these more molecular mechanisms of MS pathology, there is growing evidence supporting the role of environmental factors in the onset of MS. For example, the prevalence of MS has been shown to differ with geographical latitude, and this effect of latitude is thought to

be at least partially mediated by vitamin D [29]. Humans primary source of vitamin D is UVB radiation from sunlight, and the lower intensity of UVB radiation in certain locations may result in insufficient vitamin D synthesis [30]. Furthermore, a meta-analysis in 2014 showed an inverse association between MS prevalence and the availability of UV radiation [31]. Additionally, a number of infections have also been found to be associated with MS, especially past infection with Epstein Barr virus (EBV) [32]. Cigarette smoking has also been suggested to increase risk of MS [33, 34].

Lastly, genome-wide association studies (GWAS) and meta-analyses have identified more than 100 genomic loci that are associated with MS [35]. Genetic variants in these regions have been shown to account for approximately 30% of disease risk [29, 35].

In conclusion, although the exact aetiology remains undetermined, physiological, environmental, and genetic factors all seem to have a role in the pathogenesis of MS.

2.1.3 Diagnosis and Prognosis

MS is diagnosed via the McDonald diagnostic criteria [36], which is based on clinical assessment, laboratory testing, and magnetic resonance imaging (MRI) [37-39]. The clinical assessment, which is performed by a neurologist, includes physical examination, cognitive examination, clinical rating scales, and categorization of MS subtype. The primary rating scale used to determine the severity of MS disability is the Expanded Disability Status Scale (EDSS), which classifies patients on a mild to severe scale of 0.0-10.0 [40]. Laboratory testing is commonly completed to help rule out other potential diseases and MRI is used to assess brain and spinal cord pathology.

Based on the occurrence and pattern of MS attacks versus periods of stability, MS can be divided in to three primary subtypes: Relapsing Remitting MS (RRMS), Primary Progressive MS (PPMS), and Secondary Progressive MS (SPMS). RRMS, which is the focus of this study, is characterized by periods of relapse/attacks, when symptoms flare up for at least 24 hours, and periods of remission, when symptoms return to, or near, a baseline level. These relapses vary in frequency, duration, and severity [41]. In PPMS, there is a slow, ongoing progressive worsening of the disease that occurs right from disease onset. SPMS is characterized by an initial phase of RRMS, with at least one relapse, followed by the progressive worsening as seen in PPMS [41].

In addition to the differences between the three subtypes of MS, the prognosis of each individual subtype can be extremely variable from patient to patient. For example, some patients experience rapid worsening of symptoms within five years of diagnosis, while others patients remain at the same clinical state for 20+ years. Currently, it is extremely hard to predict prognosis in MS patients, which significantly contributes to the hardships faced by these patients, as they do not know how this disease will affect them. This results in those patients who progress more quickly not being able to fully prepare, and also causes those who may not be as severely affected to make changes and potentially sacrifices in their lives that may not have been necessary, such as deciding to not have children. Although there remains a significant gap in our knowledge about how MS progresses, ongoing research, such as the research presented here, is attempting to identify new measures of disease progression.

2.1.4 MRI in MS

As mentioned above, MRI is a critical tool for the diagnosis of MS. MRI can determine the presence and location of MS lesions, and therefore is used to evaluate if there is

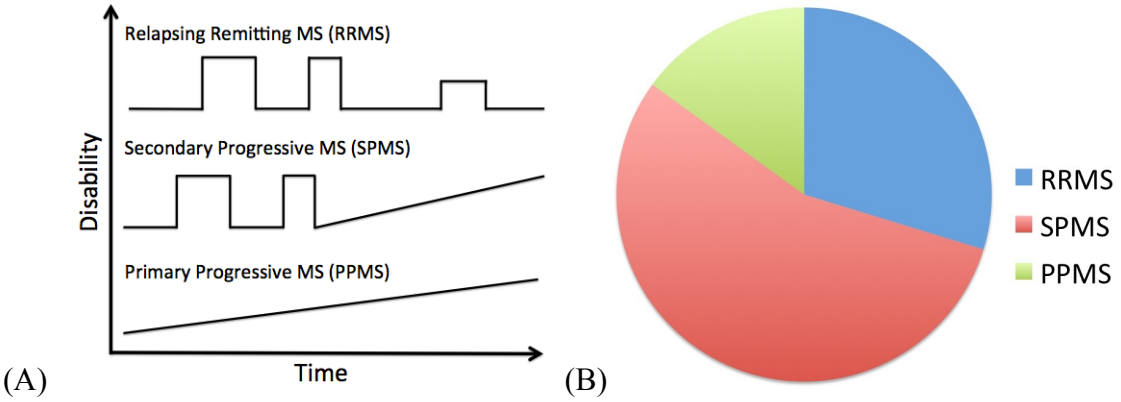

Figure 2.1: Trajectories and prevalence of the three subtypes of MS.

(A) The trajectories of the three subtypes of MS and (B) a pie chart of the percentiles of the three subtypes of MS. RRMS accounts for about 85% of MS cases at onset of the disease, but this then divides into patients who remain the RRMS subtype (about 30% of total MS cases, shown in blue in the pie chart) and patients who convert to a more progressive trajectory, referred to as SPMS (over 50% of total MS cases, shown in red in the pie chart). About 10-15% of patients (shown in green on the pie chart) present with PPMS.

dissemination of MS lesions over space and time, as this is part of the McDonald diagnostic criteria of MS [36]. MS lesions will typically appear hypointense in T1-weighted images and hyperintense in fluid-attenuated inversion recovery (FLAIR) images. Unfortunately, these radiological findings/lesions often only weakly correlate with clinical expression of the disease. For example, numerous MRI studies have shown that lesions develop up to 20 times more often than the occurrence of a clinically reported relapse. It has been suggested that this disconnect between radiological and clinical presentations of the disease may be, at least partially, due to functional reorganization, which may play a role in the recovery of disability in RRMS [42, 43]. For example, the finding that RRMS patients have more extensive and higher levels of task-induced activation has been suggested to indicate that the brains of these patients are compensating by recruiting and reorganizing neuronal activation [44]. Unfortunately, the use of BOLD fMRI alone in these studies may limit their ability to be correctly interpreted.

The research presented here investigated potential abnormalities in neurovascular hemodynamics and tissue metabolism in MS patients, which is important for accurate assessment of functional reorganization using BOLD fMRI and may also be valuable in the assessment of the progressive neurodegeneration component of the disease. We focus our attention on GM regions of interest (ROIs) because this is where fMRI responses primarily occur. Furthermore, while much of MS imaging has focused on WM pathology, it is now well known that MS also affects cerebral GM [45]; however, GM pathology is very difficult to detect with conventional MRI. There is therefore a need to better understand GM pathology and pathophysiology in MS, because it represents a significant component of the disease and may well reflect the progressive neurodegeneration component of the disease better that WM lesions. Overall, MRI has provided a solid foundation of the diagnosis and understanding of MS. Hopefully future advances in MRI, for example the approach presented in this thesis, will improve the evaluation of MS disease burden, prediction of disease prognosis, and evaluation of new treatments.

2.2 Basic Principles of Magnetic Resonance Imaging

Magnetic resonance imaging (MRI) is a non-invasive medical imaging technique that is ideally suited for neuroimaging research. It enables *in vivo* visualization of anatomy and physiology by making use of a number of physics principles and physiological phenomena.

2.2.1 Magnetism

The primary physical principle in MR imaging is the manipulation of the magnetic state of certain atomic nuclei present in tissue. Protons and neutrons have an intrinsic property known as ‘spin’, which imparts a small magnetic moment to these subatomic particles [46]. Atomic

nuclei that have an even number of protons and neutrons will generally have no net spin, as described by the Pauli Exclusion Principle; however, if a nucleus has an unpaired proton or neutron (*e.g.*, a Hydrogen atom), it will have a non-zero net spin that produces a net magnetic moment [46]. Hydrogen is the most abundant atom in the human body, making it an ideal candidate for MR imaging.

Although individual hydrogen atoms exhibit this slight magnetic moment, in a large chemical sample with an abundance of hydrogen, their magnetic fields will be randomly oriented, resulting in no net magnetization. In the presence of an externally applied magnetic field (denoted as B_0, and assumed to point along the z-direction) these hydrogen magnetic moments precess at a known frequency, referred to as the Larmor frequency, about a direction parallel or antiparallel to the externally applied field. The Larmor frequency scales linearly with the strength of the applied magnetic field. At the 3 Tesla magnetic field involved in this thesis, the Larmor frequency for a hydrogen nucleus is approximately 128 MHz, which falls within the radiofrequency (RF) band of the electromagnetic spectrum. Because the parallel precession state has a slightly lower energy compared to the antiparallel state, slightly more hydrogen nuclei (protons) will precess parallel to the magnetic field. For example, at a magnetic field of 3 Tesla, there will be approximately 10 extra parallel spins per million hydrogen atoms. Having slightly more spins in the parallel state produces a net magnetization vector (NMV) parallel to the externally applied field. The distribution of NMV is what is imaged in MRI.

After generating the NMV with the B_0 field, the application of a smaller transient rotating magnetic field perpendicular to B_0 acts to tip the NMV away from the longitudinal (z-) direction towards the transverse (xy-) plane. This second field is often referred to as an RF pulse because it is a brief burst of electromagnetic energy in the radiofrequency range rotating in the transverse

plane at the Larmor frequency. Following the application of this RF pulse, the NMV returns to the equilibrium magnetization along the z-direction after a period of time described by an exponential recovery with a time-constant referred to as T1. A longer T1 corresponds to a longer period of time required for the nuclei to return to their equilibrium magnetization. In addition to the magnetization realigning with the main magnetic field, the net transverse magnetization undergoes a rapid decay as the rotating magnetic moments (aka spins) get out of sync with each other (dephase) following the RF excitation. The rate of this transverse decay is described by time-constant T2; nuclei with a shorter T2 time constants will undergo a faster transverse decay. As this transverse magnetization rotates, it induces an electrical current in the receiver coil, producing the MR signal.

The third method for manipulating the NMV, which is required to produces images, involves the application of linearly varying spatial magnetic field gradients in the x-, y- and z-directions. These linear gradients impart a spatial dependence on the strength of the z-component of the magnetic field experienced by the spins based on their physical x-, y- and z-positions within the sample. This spatial dependence corresponds to a spatial variation in the Larmor frequency across the sample. Thus, gradients provide a method for encoding spatial information about the sample into the MR signal. This spatially sensitive MR signal is recorded in the frequency domain, also known as k-space, and reconstructed into the spatial MR image domain via the inverse Fourier transform [46].

2.2.2 Image Contrast, acquisition parameters, and pulse sequences

The primary source of image contrast between different tissues in MR images is due to the size of the NMV (aka proton density), and the different intrinsic T1 and T2 relaxation rates of

different tissue types due to their different chemical composition and microstructural configuration. The type of image contrast produced depends primarily on two factors: 1) the timing parameters of the image acquisition sequence and 2) the type of sequence. Manipulating these properties can produce images that are primarily sensitive to specific tissue magnetic properties. For example, T1-weighted and T2-weighted images were both collected for the current thesis research project. A third tissue relaxation parameter, known as T2*, is a combination of T2 decay plus additional decay caused by static magnetic field inhomogeneities experienced by the nuclei [46].

Two essential timing parameters of MR pulse sequences are the Time of Repetition (TR) and the Time of Echo (TE), both of which were chosen specifically to maximize the image contrast between tissues in data being acquired here. TR is the length of time between successive RF pulses; a portion of k-space is collected per TR. During each TR, each tissue type within the sample is undergoing T1 recovery and T2 decay. The decaying transverse magnetization can be partially refocused by either by applying a second 180-degree RF refocusing pulse, as with a spin echo (SE) pulse sequence; or by applying a series of alternating gradients, as with a gradient recalled echo (GRE) pulse sequence. The point at which the transverse magnetization is refocused is known as an echo, which occurs at time TE measured relative to the excitation RF pulse. In a SE pulse sequence, the 180-degree pulse is applied at a time of TE/2; thus refocusing the spins at time TE. This same effect can also be achieved in GRE pulse sequences by simply reversing the gradient polarity at TE/2. The choice of pulse sequence affects the type of image contrast collected from the MR data. Most MR pulse sequences can be derived from these two classes (SE and GRE). The intrinsic properties of different tissue types combined with the ability to control the timing and type of sequence enables the production of a variety of useful types of

imaging data, each with specific sensitivity to certain tissue types and pathologies. Pulse sequences with a short TR produce more T1-weighted images; conversely pulse sequences with long TE generate T2-weighted images [46].

The research presented in this thesis primarily uses a special class of GRE sequence called echo-planar imaging (EPI). Unlike typical GRE sequences that only acquire a single line of k-space per TR, EPI is a technique that can acquire an entire 2D k-space in a single TR. This reduces the time it takes to collect an image, thereby increasing the temporal resolution of the data [46]. In addition to being a fast MR pulse sequence, the signal generated with EPI can also be sensitive to small changes in the concentration of deoxyhemoglobin in the blood. As the concentration of deoxyhemoglobin increases, the apparent T2* of blood decreases, thereby lowering the corresponding EPI signal. Conversely, lower concentrations of deoxyhemoglobin produces an increase in the EPI signal. This phenomenon is known as the Blood Oxygen Level Dependent (BOLD) signal [47]. Local concentrations of deoxyhemoglobin are heavily dependent on the amount of nearby neuronal activity, due to a mechanism known as neurovascular coupling. A more comprehensive description of BOLD and neurovascular coupling is given in Section 2.3.1. The combination of its inherently high temporal resolution and this BOLD sensitivity make EPI the most commonly used sequence for fMRI.

Arterial spin labeling (ASL) is a type of MR pulse sequence technique that is sensitive to microvascular blood flow [48]. In ASL, the water molecules in the arterial blood are magnetically labeled by applying 180-degree magnetization inversion up-stream from the tissue of interest. As the labeled blood flows downstream to the tissue of interest, it exchanges with tissue water and therefore alters the MR signal from that region. The difference between images

collected with and without ASL labeling is proportional to the flow of blood (perfusion) [48, 49]. ASL is ideally suited for dynamic CBF measurements.

All fMRI data presented in this thesis were collected using a dual-echo GE-EPI (gradient echo EPI) sequence, where the data collected at the first echo is sensitive to CBF using ASL, and the data collected at the second (longer) echo is sensitive to the BOLD signal. This dual-echo GE-EPI sequence is discussed further in Section 3.3.1. As previously stated, it is the selection of the acquisition sequence timing parameters that determines the image contrast produced. The specific sequence parameters used in this thesis are discussed in more detail in Section 3.3.1.

2.3 Functional Magnetic Resonance Imaging

MRI methods for imaging MS pathology in WM continue to improve, but the lack of ability to predict disease prognosis and understand the progressive component of the disease remains a major limitation. In order to improve disease monitoring and treatment, robust biomarkers are needed for tracking GM disease progression, examining functional reorganization, and assessing the effects of treatment on GM pathology. MRI has helped explain the pathology of MS; however, its usefulness has been limited due to the discrepancy between structural MRI findings and clinical manifestations of the disease [50, 51]. fMRI enables the exploration of functional correlates of MS symptoms rather than solely looking at brain anatomy. Measures of brain function, specifically quantitative measures of cerebral physiology, may help explain how functional abnormalities of specific brain areas relate to clinical symptoms [50].

2.3.1 Blood-Oxygen-Level-Dependent fMRI

fMRI offers a sensitive, non-invasive technique to localize brain activity, and can be used to gain information about how the brain functions in the presence of MS pathology. A healthy brain generally responds to an external stimulus in a fairly predictable way: upon presentation of a stimulus or execution of a task, an increase in neural activity is coupled with an increase in blood flow (called the hemodynamic response), and this increase in blood flow produces a BOLD fMRI signal. See **Figure 2.2** for a visual representation of this process.

Neural activity involves the production and transmission of action potentials, which are transient events whereby the polarity of the cell membrane changes and an electric signal is sent along the axon of the cell (shown in **Figure 2.3**). This physiological mechanism is significantly disrupted in MS, as myelin is essential to the rapid transduction of action potentials. The demyelination that occurs in MS impairs the ability of neurons to transduce action potentials, therefore impairing the function of these neurons.

fMRI is generally based on BOLD contrast that arises from focal changes in deoxyhemoglobin concentration during changes in neural activity [47, 52, 53]. The production of adenosine triphosphate (ATP), which maintains all cerebral activity, is primarily sustained through aerobic metabolism [54, 55]. The increase in oxygen metabolism associated with increased neuronal activity requires an increase in blood flow to increase the supply of oxygen and glucose; this constitutes the physiological basis of the BOLD contrast. In healthy subjects, during neural stimulation, cerebral blood flow (CBF) and the cerebral metabolic rate of oxygen consumption ($CMRO_2$) increase in a correlated manner, but CBF increases in excess of $CMRO_2$ [56]. This overcompensation of CBF results in an increase in oxygenated blood in activated areas of the brain. Deoxygenated hemoglobin is paramagnetic; therefore, it interacts with the magnetic

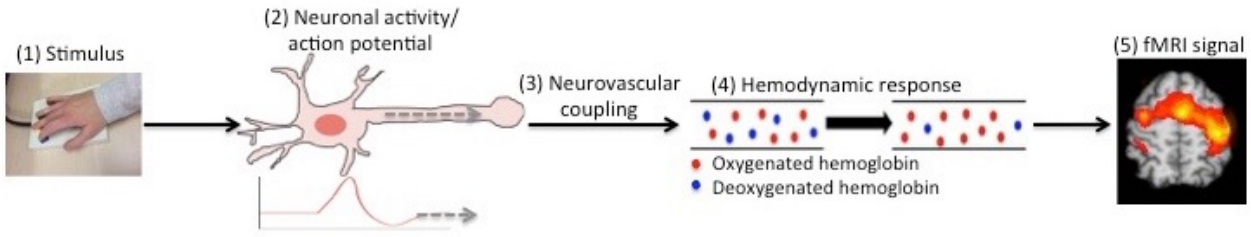

Figure 2.2: The physiological process of a neuron responding to a stimulus.
A stimulus, such as a finger-tapping motor task (1), elicits an increase in neural activity in the area of the brain responsible for that task (2). This neural response is coupled to a vascular response (neurovascular coupling) (3), which causes an increase of blood flow to that area of the brain (hemodynamic response) (4). This increase in the ratio of oxygenated haemoglobin to deoxygenated haemoglobin produces the fMRI signal (5) because oxygenated haemoglobin is diamagnetic, so interferes with the MR signal less than deoxygenated haemoglobin, which is paramagnetic. (Figure adapted from [57])

field and decreases the MR signal. Oxygenated hemoglobin is slightly diamagnetic (similar to tissue) so does not decrease the MR signal. When an area of the brain is activated in a healthy subject, the ratio of oxygenated hemoglobin to deoxygenated hemoglobin in the blood vessel will increase, and the BOLD fMRI signal in this brain area will therefore also increase [47, 52, 53], as shown in **Figure 2.2**.

In MS, conventional BOLD fMRI studies have shown increased responses during motor tasks, relative to controls [43, 58-60]. In response to a unilateral hand motor task, increased BOLD responses have been observed in MS in the ipsilateral motor and premotor regions [44, 61], and in the ipsilateral inferior parietal lobe [44]. Furthermore, MS patients with severe fatigue appear to have greater activation in different areas than MS patients without severe fatigue. Patients with fatigue have been shown to have greater activation than patients without fatigue in the right premotor area, the putamen, and the dorsolateral prefrontal cortex. Patients

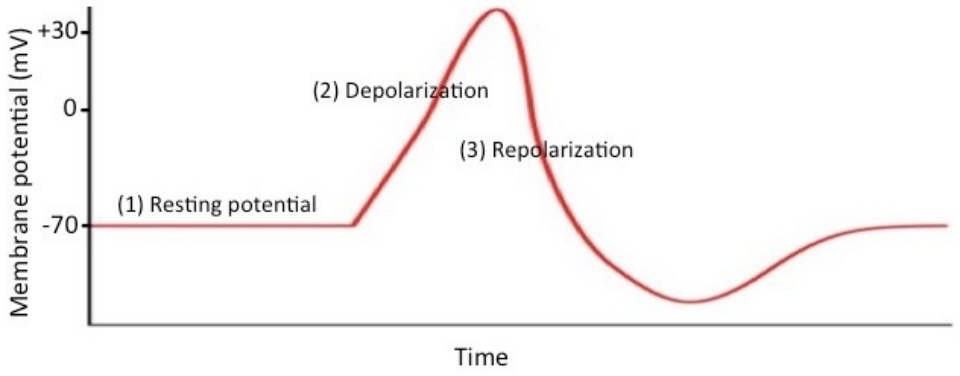

Figure 2.3: Schematic of an action potential.

The membrane of an inactive neuron has a typical resting potential of around -70 mV (1). When the neuron is excited, the membrane becomes depolarized to around +40 mV (2) and the action potential travels down the neuron's axon. Once the neuron is completely depolarized, it undergoes repolarization (3) to reset its membrane potential back to resting, in preparation for another action potential.

without fatigue, on the other hand, show greater activation in the left and right primary sensorimotor cortex, the right supplementary motor area, the left premotor cortex, and the left cerebellum [58]. In addition to the recruitment of extra regions, the BOLD response amplitude in the expected cortical regions is also increased in MS compared to controls [42]. For example, during execution of a simple motor task, MS patients have been shown to exhibit significantly more BOLD activations in fronto-parietal regions, as compared to healthy controls [62]. Although the focus of this thesis is the motor network, it is important to note that MS patients have also been shown to have higher levels of activation in brain regions other than the motor network, for example in cognitive networks [63].

It has been suggested that this increased cortical recruitment is adaptive for patients with MS [64]. It is thought that higher levels of activation and activation of additional regions is a compensatory mechanism, which is required to complete the same task as healthy controls [60]. The ability to compensate may limit the clinical severity of MS [60]. This conclusion is

predicated on the assumption that task-induced BOLD changes are accurately reflecting changes in neural activity. However, this assumption is not necessarily true, especially in pathological conditions such as MS.

As discussed earlier, the BOLD signal is not a direct measure of neural activity, but rather relies on the relative changes in $CMRO_2$ and CBF, as well as cerebral blood volume (CBV) [65]. Though the BOLD signal has provided great insight into MS, the complex and indirect nature of BOLD fMRI limits its clinical application. Furthermore, the physiological processes underlying the BOLD response have been reported to be abnormal in MS [1-3], suggesting that a significant amount of observed BOLD differences in MS patients might be explained by other physiological abnormalities.

2.3.2 Cerebrovascular Measures in fMRI

Cerebrovascular reactivity (CVR), which is a key measure of cerebrovascular health, is the ability of the cerebrovasculature to respond to vasodilatory stimuli by modulating CBF and cerebral blood volume (CBV). CVR can be measured by quantifying the change in BOLD or the global change in CBF caused by a global vasodilator. Global BOLD measurements can be obtained from conventional BOLD fMRI, as discussed above, and continuous CBF measurements can be obtained using ASL.

Cerebral Blood Flow

CBF has been reported to be abnormal in MS; however, results are not consistent between studies. Baseline global grey matter (GM) CBF has been reported to trend higher (non-significant) in MS patients compared to healthy controls [1]; however, a global CBF decrease in

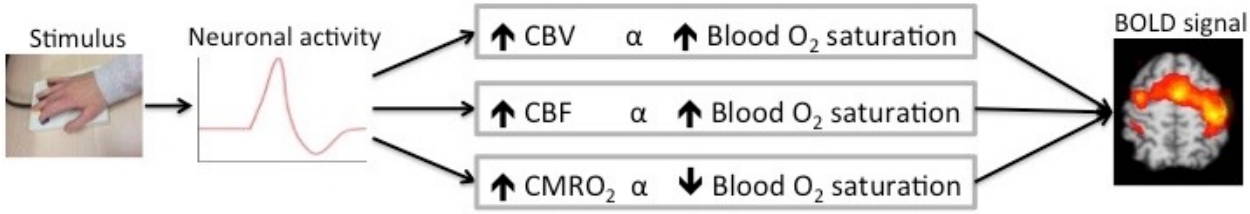

Figure 2.4: Neurophysiology of the BOLD response.

As in Figure 2.2, a stimulus evokes an increase in neural action potentials, which causes an increase in CBV, CBF, and $CMRO_2$. CBF and $CMRO_2$ are coupling together (neurovascular coupling) such that the increase in CBF is larger than the increase in $CMRO_2$, resulting in a net increase in blood O_2 saturation. The BOLD response produces by the increase in neural activity is dependent on the stimulus-induced change and also the baseline level of all of these underlying physiological mechanisms. (Figure adapted from [66])

normal-appearing white matter (NAWM) and GM has also been reported in MS [2]. CBF may also differ between MS subgroups [67]. One study found that some GM regions in PPMS and SPMS have lower perfusion compared to controls, whereas some WM regions in RRMS and SPMS have comparatively higher perfusion [67]. Furthermore, in a comparison between high- and low-inflammatory RRMS patients (according to the number of new active lesions), the high-inflammatory group had significantly higher CBV and CBF values in the NAWM [68]. Additionally, differences in perfusion in RRMS lesions have been shown to depend on whether the lesion is active or not [69]. Compared with normal white matter, T1-hypointense lesions (i.e. non-active lesions) show lower perfusion, whereas gadolinium-enhancing lesions (i.e. active lesions) appear to have increased perfusion [69]. Taken together, more research is needed to clarify the presence of CBF abnormalities in MS.

Cerebrovascular Reactivity

The task-induced change in CBF and in BOLD is dependent on CVR, which is the dilatory ability of the blood vessels. CVR has recently been reported to be abnormal in MS [1]. Marshall et al. conducted a study using ASL-based CBF to measure CVR in 19 healthy controls compared to 19 MS patients; the patient group had a mean (SD) EDSS score of 2.9 (1.5). Global GM CVR was found to be lower in patients with MS compared to healthy controls [1]. Regionally, MS patients had lower CVR in more than 25% of the GM volume of the superior temporal gyri, supramarginal gyri, rolandic opercula, Heschl gyri, anterior cingulate gyri, and lenticular nuclei [1]. These CVR measurements were negatively correlated with lesion volume and brain atrophy [1]. Transcranial Doppler (TCD) has also been used to assess CVR in RRMS patients during an MS attack (mean EDSS = 2), as well as after treatment during a period of remission (mean EDSS = 1); however, this study did not find significant CVR differences between controls and patients at either stage [70]. These contradicting results may be due to methodological differences. TCD measures blood velocity in larger arteries rather than measuring tissue perfusion, as is measured with MRI based ASL. We measured CVR using two techniques: BOLD-CVR and CBF-CVR; the results provide additional information about whether CVR is impaired in MS.

2.3.3 Oxygen Metabolism Measures in fMRI

Mitochondria are aerobic cellular organelles that produce energy and regulate cellular metabolism; it has been suggested that mitochondrial damage contributes to neurodegeneration in MS [71]. Oxidative stress, which is caused by an uncontrolled increase in reactive oxygen

species (ROS), has been documented in inflammatory MS lesions [72, 73]. This inflammation-derived oxidative stress may damage nearby mitochondria [73]. Regardless of the cause, mitochondrial dysfunction may play a role in the pathophysiology of MS. Specifically, because mitochondria require oxygen to function, decreased mitochondrial activity may directly relate to $CMRO_2$, therefore motivating its investigation.

Although there is currently little known about $CMRO_2$ in MS patients, one study, which used a whole brain measurement technique called T2-relaxation-under-spin-tagging (TRUST) and phase contrast velocity imaging, found significantly lower baseline whole-brain $CMRO_2$ in MS patients compared to healthy controls [3]. $CMRO_2$ was also negatively correlated with both EDSS and lesion load [3]. Global oxygen extraction fraction (OEF), another measure of oxygen consumption, was reported to be reduced in patients with MS [74]. These findings demonstrate the importance of characterizing $CMRO_2$ in MS patients in order to advance the current understanding of MS pathophysiology and help explain BOLD observations in MS.

2.3.4 Flow-Metabolism Relationship

Similar to individual physiological processes affecting BOLD, the BOLD response is also dependent on a phenomenon called neurovascular coupling. Neurovascular coupling is the link between neural activity and the associated change in CBF; therefore, this coupling ratio is a critical component of the BOLD phenomena. Although fMRI cannot directly measure neural activity, relative changes in $CMRO_2$ can be estimated (as outlined in Section 3.4.3) and used to represent neural energetic workload. Quantifying the flow-metabolism relationship ($\Delta CBF/\Delta CMRO_2$) therefore provides a way to investigate this coupling mechanism. In healthy subjects, CBF and $CMRO_2$ have a linear relationship [75] with a ratio typically between 2:1 and

4:1 ($\Delta CBF:\Delta CMRO_2$) [76-79]. As discussed earlier, the fact that this ratio is greater than 1 leads to the phenomenon of focal hyperemia that gives rise to the positive BOLD fMRI signal.

In addition to explaining pathophysiology, identifying if there are abnormalities in the flow-metabolism relationship in MS patients can help clarify the occurrence of abnormal BOLD responses seen in these patients. Without characterizing the individual components that contribute to the BOLD signal, fMRI data may be incorrectly interpreted. For example, an abnormally high $\Delta CBF/\Delta CMRO_2$ ratio could result in large BOLD responses despite normal neural activity. This is especially important for patient populations, such as MS, in which cerebral hemodynamics, CVR, and the flow-metabolism relationship, may be abnormal.

2.3.5 Quantitative fMRI

Due to the cerebral physiological abnormalities reported in the MS literature, BOLD results alone cannot be used to fully characterize the underlying neural activity in MS. Abnormal BOLD responses detected in MS may not reflect neural activity, but rather, may reflect abnormalities in the physiological processes that make up the BOLD response. The existence of these abnormalities, as well as the ambiguity of past fMRI results, have motivated the application of new quantitative fMRI techniques to help understand the GM pathophysiology of MS.

Quantitative fMRI techniques have been developed to study the physiological basis of BOLD fMRI in healthy subjects. These techniques include evaluations of CBF using ASL [48, 49, 80], CVR using ASL and BOLD, and $CMRO_2$ using the calibrated BOLD model [81-85]. Quantitative measures are especially insightful in patient populations with compromised cerebral hemodynamics or metabolism. This study therefore used quantitative fMRI techniques to study

the MS brain, investigating the presence of global GM impairments, and more specifically looking at the motor networks of the brain.

2.3.6 Motor Impairment in MS

Motor impairments are one of the most common and disabling symptoms of MS. Within 10 years of diagnosis, 30% of MS patients require the use of a walking aid, and within 30 years of diagnosis, this increases to 80% of patients [86]. Numerous questions relating to MS pathology and motor deficits remain unanswered. As previously discussed, BOLD studies often report a larger task-induced neural response in the motor networks of MS patients compared to healthy controls. This increased BOLD response represents an increase in the oxygen saturation of blood in the motor network; however, is not a direct measure of the neural response. The collection of quantitative fMRI measures during a motor task enables the hemodynamic and metabolic components of the BOLD responses to be disentangled.

The present study focused on upper limb function, as about 75% of MS patients experience upper limb movement deficits during the disease course [11]. In addition to data collection for a conventional motor execution (ME) task, data was also collected for a motor imagery (MI) task. Imagery involves the performance of movement without physically executing movement; therefore, successful completion of an MI task does not rely on motor function. MI tasks activate many of the same brain areas as ME tasks in healthy controls [4]. If MI activates similar brain regions as ME in MS patients, MI can be used to investigate fMRI measures irrespective of the patient's hand motor function. Additionally, voxel-wise analysis of ΔBOLD and ΔCBF fMRI data during a ME task versus a MI task provides the groundwork for

investigation of the future applicability of MI tasks in MS and possibly other neurological conditions, such as stroke.

2.3.7 Summary

fMRI research on MS is currently limited because of the ambiguity of BOLD measurements in pathology. Abnormalities have been identified, but the details of the underlying pathophysiology remain unclear. The quantitative fMRI measures investigated in this thesis can provide new insights about the cerebral physiological underpinnings in MS. Specifically, we investigated two primary measures: (1) the flow-metabolism relationship in the cerebral motor network, and (2) global GM cerebrovascular reactivity. By quantifying the flow-metabolism relationship and its underlying parameters, including BOLD, CBF, and $CMRO_2$, this thesis helps explain the physiology of the BOLD response in MS patients, and provides further explanation of existing literature that suggests BOLD is altered in MS patients. Additionally, the findings of this thesis warrant future exploration of the potential of these measures as novel biomarkers of MS GM pathology and/or of treatment efficacy.

Chapter Three: Methods

3.1 Description of the Study Population

After obtaining approval from the research ethics board (Ethics ID: REB14-2431), sixteen MS patients and fifteen age- and sex-matched healthy controls were recruited to participate in this study. All participants provided written informed consent at the beginning of their appointment. Study participants were recruited according to the following criteria:

(1) Patient group: MS patients were recruited through the Calgary MS Clinic, based out of Foothills Hospital. To be considered for the study, patients had to meet the following inclusion criteria: 1) diagnosis of clinically definite RRMS (as defined by the revised McDonald criteria [39]; 2) an EDSS (Kurtzke's Expanded Disability Status Scale [87]) score of 0 to 6.5; 3) aged 18-65, 4) ability to perform sequential finger tapping motor execution and motor imagery; 5) right-handed; and 6) visual acuity sufficient to view visual stimuli (or correctable using MRI-compatible lenses). The following were used as exclusion criteria: 1) any neurological disease other than MS; 2) occurrence of a relapse within one month prior to the study appointment; 3) severe respiratory syndrome (COPD, uncontrolled asthma, lung cancer, etc.); 4) severe cardiovascular disease; 5) seizure disorder; 6) taking baclofen; 7) daily smoking; 8) claustrophobia or other contraindications for an MRI exam (e.g., pacemaker); and 9) pregnancy.

(2) Control group: The inclusion criteria for controls were: 1) no history of any neurological disease; 2) aged 18-65; 3) ability to perform sequential finger tapping motor execution and motor imagery; 4) right-handed; and 5) visual acuity sufficient to view visual stimuli (or correctable using MRI-compatible lenses). The same exclusion criteria listed for the MS patients were also applied to healthy controls.

Participants were initially screened over the phone prior to scheduling an appointment, and were screened again on the day of their appointment.

This study only included MS patients with the relapsing-remitting subtype in order to reduce variability in the patient group, enable comparison with the existing literature on fMRI in RRMS. Additionally, the patients were studied during a period of remission to investigate cerebral abnormalities that are not directly associated with acute MS attacks.

The full data sets of five patients and three healthy controls were retrospectively excluded due to a variety of factors affecting imaging data quality. This is discussed in more detail in section 3.4.1.

The remaining eleven patients (seven females and four males) had a mean (SD) age of 51.7 (8.3) and the remaining twelve controls (10 females and 2 males) had a mean (SD) age of 49.3 (8.6). The patient group had a mean (SD) EDSS score of 2.3 (1.1), ranging from 1-4, and a mean (SD) disease duration of 16 (11) years, where disease duration was defined as the time period (in years) between clinical diagnosis and the participant's research appointment. Of the eleven patients, eight were on immunomodulating treatments (three on Tecfidera, three on Copaxone, one on Rebif, and one on Aubagio). Additionally, three patients were on anti-depressants (one on Pristiq, one on Effexor, and one on Fluoxetine), one patient was on Detrol to treat bladder muscle spasms, one patient was on Tecta to reduce stomach acid, one patient was on Lyrica, and two patients were on Synthroid for hypothyroidism. Of the twelve controls, three were on anti-depressants (two on Effexor and one on Clomipramine) and one was on Norvasc for high blood pressure.

3.2 Experimental Design

3.2.1 Hypercapnia Paradigm

For the hypercapnia condition, a gas mixture consisting of 5% CO_2 and 95% medical air was administered through a breathing circuit (**Figure 3.1A**). The CO_2 gas mixture was administered for two minutes, preceded and followed by medical air for two minutes (**Figure 3.1C**). The delivery of gases was controlled by Digital FloBox model 954 (Sierra Instruments, Monterey, CA, USA) via the SideTrak® 840 Analog Gas Mass Flow Controllers (MFCs; Sierra Instruments, Monterey, CA, USA). The *GasSequencer* program was used to send commands to Flo-Box to maximize accuracy of the timing of gas delivery. Lumina Box Controller (Cedrus, San Pedro, CA, USA) enabled the gas delivery computer to receive scanner triggers to ensure the timing of the gas delivery was in sync with the MR scan. For the duration of the hypercapnia task, end-tidal partial pressures of CO_2 and O_2 were continuously sampled (see sampling line in **Figure 3.1B**) using CO2100C (for CO_2) and O2100C (for O_2) modules for MP150 system (Biopac Systems Inc., Goleta, CA, USA) accompanied by the Acqknowledge software program (Acqknowledge 4.4; Biopac Systems Inc., Goleta, CA, USA).

3.2.2 Motor Task Paradigm

The task condition, based primarily off of similar established block designs [88, 89], consisted of two motor tasks, ME and MI. Both tasks were performed unilaterally by the right hand only. The ME condition involved button pressing with the right hand fingers in the following repeating sequence: index finger, ring finger, middle finger, pinky finger. A flashing black cross was presented on the MR projector screen to cue participants to press the buttons at a frequency of 1Hz. The MI condition involved the same 1Hz flashing cross, but participants were asked to imagine the kinaesthetic feeling of the button-pressing action without making any

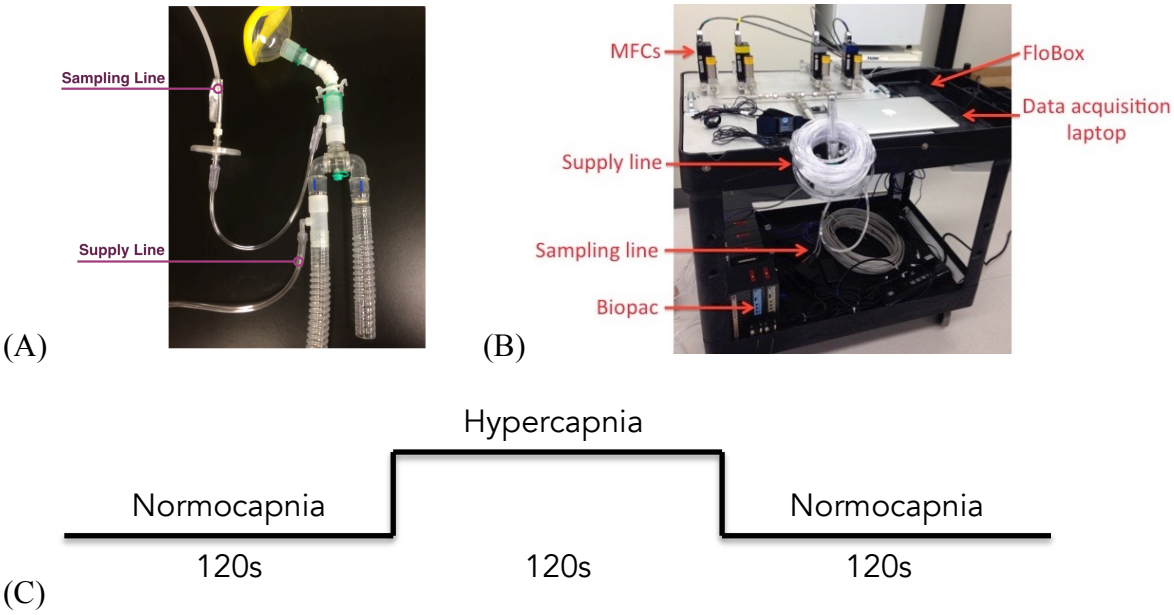

Figure 3.1: Gas challenge breathing circuit, cart, and design.

(A) The breathing circuit – the participant's mouth and nose are covered by the yellow mouthpiece, which is secured to their head with elastic fasteners (not shown), (B) the gas delivery system cart, and (C) the design of the hypercapnia condition, where hypercapnia is a state of excessive CO_2 in the bloodstream, and normocapnia is normal CO_2 pressure in the bloodstream.

physical movement. For the MI condition, an emphasis was placed on that participants should focus on imagining what the movement would feel like if they were doing it, i.e. first person, rather than imagining seeing someone do the movement. A block paradigm was used such that ME and MI blocks were altered with rest blocks (**Figure 3.2**). In the middle of each ME or MI block, the participant was cued with the word 'restart' to briefly pause their tapping and resume tapping when the cross started flashing again, starting tapping with the index finger. This restart command has been commonly used in previous motor tasks [88, 89] to attempt to increase the participant's attentiveness. The restart command also allowed participants to start over if they lost their place or made a mistake. Furthermore, at the end of each motor block, participants were

(A)  (B) 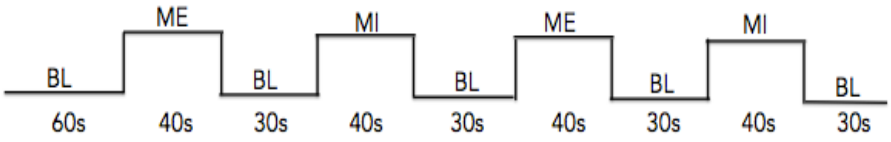

Figure 3.2: The motor task pad and block design.

(A) The motor pad used for the motor task (LU444-RH, Cedrus, San Pedro, CA, USA) and (B) the block design of the motor task. As shown here, one run of the motor task consisted of two 40-second ME blocks and two 40-second MI blocks. Each participant completed two full runs, for a total of four blocks of each condition. ME = motor execution; MI = motor imagery; and BL = baseline.

cued to press the next finger in the series. This response was required for both the ME and MI blocks, and allowed the participants MI performance to be evaluated in the absence of overt movement. The visual cues for the motor tasks were presented using PsychoPy [90]. A MR safe video camera (12M camera, MRC Systems GmbH, Heidelberg, Germany) was used to monitor the hand movements of participants, and to ensure participants were not making overt movements in the MI task blocks.

3.3 Study Protocol

After providing written informed consent, participants were fully screened to ensure it was safe for them to participate in the study and receive an MRI.

A blood sample (3ml) was collected at the Heritage Medical Research Clinic in the Teaching, Research and Wellness centre at Foothills Hospital. Calgary Lab Services tested the blood samples for hematocrit and haemoglobin concentration. These values were used to account for individual differences between participants.

After the blood draw, participants underwent motor and cognitive testing. The motor function tests consisted of the Timed 25-Foot Walk (T25-FW) and the 9-Hole Peg Test (9-HPT), which are two components of the Multiple Sclerosis Functional Composite [91]. The T25-FW is a measure of mobility and leg function; it requires the subject to walk 25 feet as fast and safely possible [92]. The 9-HPT is a measure of upper extremity function; it requires the subject to insert 9 pegs into 9 holes and then remove them as quickly as possible. After the motor function testing, cognition was assessed using the Symbol Digit Modalities Test (SDMT) [93]. The SDMT requires the examinee to pair abstract symbols with specific numbers; this task involves numerous components of cognition, including attention, working memory, and visuoperceptual processing [93]. The T25-FW, 9-HPT, and SDMT were administered by a trained researcher (JB). Participants also completed the Modified Fatigue Impact Scale (MFIS) [94] and Mental Health Inventory (MHI) [95] questionnaires. Data from these assessments was used to characterize the sample and control for inter-subject variability in these domains. After completion of the above assessments, participants were trained on the ME and MI tasks that they were to perform during the MRI scan.

The MRI scanning was performed at the Seaman Family MR Research Centre. The participants' blood pressure was also taken at the Seaman Family MR Research Centre. At the end of the appointment, participants completed a short debriefing form, where they were able to share what they liked and did not like about participating in the research study.

Additionally, demographic and basic health information (i.e., medications, education level, caffeine intake, sleep, etc.) was obtained from a questionnaire, and was used to reduce participant-specific confounds.

3.3.1 MRI Protocol

Magnetic resonance imaging was performed on a 3.0 Tesla GE scanner (Discovery 750, General Electric Healthcare, Waukesha, WI) using a 12-channel receive-only head coil. A dual-echo EPI pseudo-continuous ASL (pCASL) sequence, with Array coil Spatial Sensitivity Encoding (ASSET) turned on, was used to simultaneously acquire CBF and BOLD measurements, acquired at echo 1 and echo 2, respectively, during hypercapnia and the motor tasks. Acquisition parameters included: TR = 3500 ms, TE1 = 9.5 ms, TE2 = 30 ms, interleaved tag and control images, post-labeling delay = 900 ms, and labeling duration = 1600 ms. An in-plane spatial resolution of 3.5 mm x 3.5 mm was used, with 18 slices and a slice thickness of 5 mm (1 mm slice gap). The labeling location was selected to be 20mm inferior to the most inferior imaging slice (**Figure 3.3**).

In addition to the above 18-slice dual-echo pCASL acquisition, the same sequence was also used to acquire a whole brain 28-slice image. This whole brain functional image was used to register the other functional images to the anatomical image.

A T1-weighted structural scan was acquired for anatomical reference and spatial normalization (BRAVO sequence, 1 mm^3 isotropic voxel size). Additionally, each MRI session included a 3D T2-FLAIR (fluid-attenuated inversion-recovery), which is sensitive to cerebral pathology, such as MS lesions.

Figure 3.3: The ASL labeling location.

The labeling plane (solid red line) was manually positioned 20mm below the bottom of the imaging slab (dashed blue line) for the dual-echo pCASL sequence.

3.4 Data Analysis

3.4.1 Image Processing

Prior to any processing, all imaging data underwent GE's Phased array Uniformity Enhancement (PURE) to minimize surface coil intensity variations.

Image analysis was performed primarily in FMRIB Software Library (FSL) [96], but in-house software and additional third-party packages, such as Statistical Parametric Mapping 8 (SPM8) (Wellcome Trust Centre for Neuroimaging, London, UK) [97], were also used. FSL was chosen as the primary software package in order to maintain consistency within the lab and with other researchers in this field [55, 98, 99]. Furthermore, FSL has been shown to minimize intersession variability more than SPM when analyzing time-series statistics [100].

The interleaved dual-echo data was separated into an echo 1 (ASL) 4D image and an echo 2 (BOLD) 4D image. Raw data was preprocessed, including motion correction and spatial smoothing (5mm full width at half max (FWHM) Gaussian kernel), in the ASL Data Processing

Toolbox in SPM [101, 102]. Data runs with more than 3 mm of motion were excluded from further analysis. Non-brain structures were removed from anatomical and functional images using the Brain Extraction Tool (BET) with the bias field and neck cleanup option in FSL [103]. Echo 1 ASL data underwent control-tag subtraction using sinc temporal interpolation to generate a perfusion-weighted time series with the same sampling rate as the original time series [104]. Image registration was performed in the FSL toolbox FLIRT [105, 106]. The functional data from the hypercapnia run and two motor runs were first registered to the low resolution whole brain functional image using a linear transform with 3 degrees of freedom (DOF), which was then registered to the high resolution structural image using a linear Boundary Based Registration (BBR) [107]; this in turn was registered to Montreal Neurological Institute (MNI) standard space [108, 109] using a linear transformation with 12 DOF. After preprocessing the data, statistical analyses of functional data were completed in the FEAT FSL toolbox [110].

In the FEAT toolbox [110], a general linear model (GLM) was used to model the effects of hypercapnia on BOLD (echo 2 time series) and CBF (perfusion time series generated as described above). The 5% CO_2 gas administration time course was convolved with a gamma hemodynamic response function (standard deviation = 15s, mean lag = 30s) [111] and then fit to the BOLD and CBF data in a voxel-wise analysis.

Similarly, to model the effects of the motor tasks (ME and MI) on BOLD and CBF, the time course of the motor task block design was convolved with a gamma hemodynamic response function (standard deviation = 3s, mean lag = 6s) and analyzed in the GLM. For each participant, the following six t-contrasts were calculated for BOLD and CBF for both motor runs: ME-induced increased activation, ME-induced decreased activation, MI-induced increased activation, MI-induced decreased activation, ME-induced activation > MI-induced activation, and MI-

induced activation > ME-induced activation. Clusters of activated voxels were detected using z-stat > 2.3 and a corrected significance threshold of $p = 0.05$ [110]. All fMRI maps were corrected for multiple comparisons using cluster-based thresholding ($p < 0.05$).

In addition to the voxel-by-voxel analyses, the average percent signal change of CBF and BOLD responses for each run (hypercapnia and two motor runs) were generated for three distinct ROIs, which are defined below.

3.4.2 ROI Selection

The Juelich histological atlas was used to create region of interest (ROI) masks for the left premotor cortex (BA6), the left primary motor cortex (BA4), and the left primary somatosensory cortex (BA1-3) [112-114]. Juelich probabilistic maps of each of these ROIs were thresholded to include only those voxels identified as having a 50% or greater probability of belonging to the respective ROI; ROIs were then binarized (**Figure 3.5**). These structural ROIs were then further restricted by the intersection of statistically thresholded subject-level BOLD (z-stat > 2.3 and cluster p-threshold = 0.05) and statistically thresholded subject-level CBF (z-stat > 2.3 and cluster p-threshold = 0.05) images of both the hypercapnia and motor runs. Additionally, ROIs consisted of GM only. FMRIB's Automated Segmentation Tool (FAST) was used to segment GM for each ROI as well as create a whole brain GM mask [115].

(A)

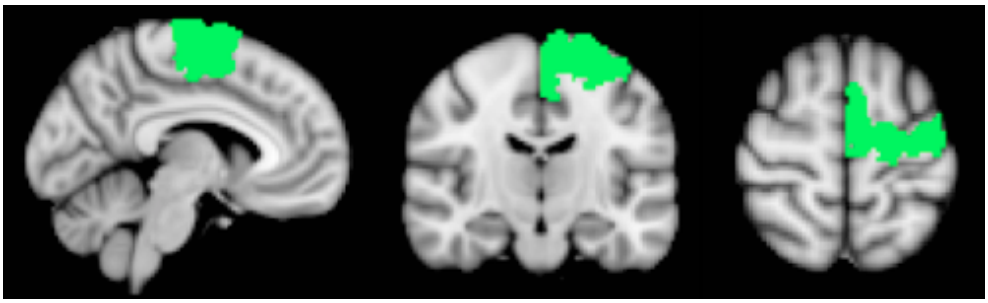

(B)

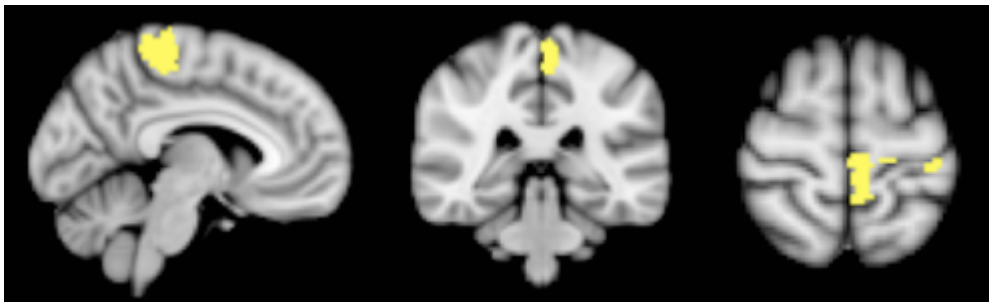

(C)

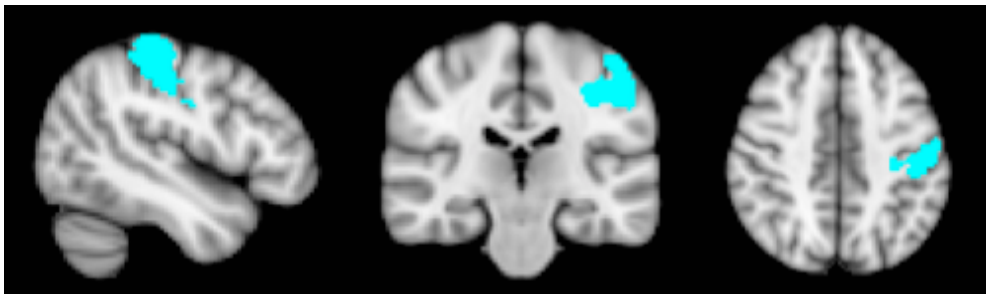

Figure 3.4: Anatomical boundaries for the three ROIs.

These anatomical ROIs were then further restricted using subject-level functional data, as described above. The three ROIs, including the left premotor cortex (A), left primary motor cortex (B), and primary somatosensory cortex (C), were obtained from the Juelich histological atlas (source).

3.4.3 Subject-level Statistical Analysis

In addition to the previously discussed subject-level voxel-wise analysis, the average percent signal change (psc) of CBF and BOLD responses was generated for each ROI for the following two t-contrasts: ME > baseline and MI > baseline. Average BOLD psc and CBF psc were also calculated for the hypercapnia condition (hypercapnia > normocapnia), as these

averages are necessary to determining CVR, as well as the average psc of $CMRO_2$ in the three ROIs as discussed below.

Determining ΔCMRO₂ and the flow-metabolism ratio

Task-induced changes in $CMRO_2$ were calculated using previously determined methods [84], which model $\Delta CMRO_2$ based on BOLD and CBF signals. This model, later named the deoxyhemoglobin dilution model [85], can be represented as the following:

$$\frac{\Delta BOLD}{BOLD_0} = M\left(1-\left(\frac{CMRO_2}{CMRO_{2|0}}\right)^{\beta}\left(\frac{CBF}{CBF_0}\right)^{\alpha-\beta}\right) \qquad (1)$$

The β value is a constant in the range $1 < \beta < 2$, which accounts for variations in the deoxyhemoglobin concentration dependence of relaxivity (R_2*) [116]. A β-value of 1.3 was used in this study, as is typically used for calibrated BOLD studies at 3 T [117]. The parameter α accounts for the power-law relationship between CBF and CBV [118],

$$\frac{CBV}{CBV_0} = \left(\frac{CBF}{CBF_0}\right)^{\alpha} \qquad (2)$$

Based on previous research, α has been set to be 0.2 [119]. The M parameter in the deoxyhemoglobin dilution model (equation 1) represents the maximum possible BOLD response, which is the BOLD response that would result from removal of all venous deoxyhemoglobin [84]. The value of M was estimated using a physiological hypercapnia challenge. Increasing the arterial partial pressure of CO_2 ($PaCO_2$) causes a global dilatory response of cerebral blood vessels [120], causing a change in BOLD, CBV, and CBF [58]. $CMRO_2$ has been shown to remain stable during mild to moderate hypercapnia [121]. BOLD and

CBF were measured at baseline and during hypercapnia. These measurements and the assumed values for α and β were then used to calculate M:

$$M = \frac{\Delta BOLD}{BOLD_0}\left(1 - \frac{CBF^{\alpha-\beta}}{CBF_0}\right)^{-1} \qquad (3)$$

Using the calculated M-value, the task-induced change in $CMRO_2$ was calculated as follows:

$$\frac{CMRO_2}{CMRO_{2|0}} = \left(1 - \frac{\left(\frac{\Delta BOLD}{BOLD_0}\right)}{M}\right)^{1/\beta} \left(\frac{CBF}{CBF_0}\right)^{1-\alpha/\beta} \qquad (4)$$

where the BOLD and CBF values are determined during the task activation condition. $\Delta CMRO_2$ was calculated for each of the previously defined ROIs.

The calculated activation induced $\Delta CMRO_2$ was then compared to the respective changes in CBF to determine the flow-metabolism ratio in each ROI in both task runs for each subject.

Determining cerebrovascular reactivity

CVR was calculated using two techniques: BOLD-CVR and CBF-CVR. BOLD-CVR was calculated as the psc of the BOLD response during hypercapnia divided by the change in end-tidal CO_2 ($ETCO_2$) partial pressure, as shown below:

$$\mathrm{CVR_{BOLD}(\%/mmHg)} = \frac{100 \text{ x } (\mathrm{BOLD_{hypercapnia}} - \mathrm{BOLD_{normocapnia}})/\mathrm{BOLD_{normocapnia}}}{\mathrm{ETCO_{2,hypercapnia}} - \mathrm{ETCO_{2,normocapnia}}} \qquad (5)$$

Similarly, CBF-CVR was calculated as the psc of CBF during hypercapnia divided by the change in $ETCO_2$:

$$\mathrm{CVR_{CBF}(\%/mmHg)} = \frac{100 \text{ x } (\mathrm{CBF_{hypercapnia}} - \mathrm{CBF_{normocapnia}})/\mathrm{CBF_{normocapnia}}}{\mathrm{ETCO_{2,hypercapnia}} - \mathrm{ETCO_{2,normocapnia}}} \quad (6)$$

3.4.4 Group-level Statistical Analysis

Within-group voxel-wise Analysis of BOLD and CBF

FMRIB's Local Analysis of Mixed Effects (FLAME) was used for voxel-wise within-group and between-group repeated measures analyses of task-induced ΔBOLD and ΔCBF activation [122-124]. The effect of task was analyzed at the voxel-wise level for task-induced ΔBOLD and task-induced ΔCBF in order to determine if MI can be used to investigate the motor network in MS patients. This analysis was completed in FEAT using FLAME [122-124].

Within- and Between-group ROI analysis of flow-metabolism ratio, $CMRO_2$, BOLD, and CBF

For all task data, after the first-level analysis on individual task runs was complete, a linear mixed effects analysis was conducted for each ROI, for all fMRI measures, including baseline BOLD, baseline CBF, task-induced ΔBOLD, task-induced ΔCBF, task-induced $\Delta CMRO_2$, and the flow-metabolism ratio. The mixed effects analysis allowed the evaluation of the main effect of group (MS versus HC) and the main effect of task (ME versus MI). Additionally, the presence of an interaction effect between task and group was tested for. All measures were Bonferroni corrected for multiple comparisons.

Between-group voxel-wise Analysis of Cerebrovascular Reactivity

Voxel-wise between-group analyses of hypercapnia-induced BOLD and CBF activation maps were also completed using FLAME [122-124]. Grey matter BOLD-CVR and CBF-CVR,

quantified using whole brain GM masks at the individual level, were compared between groups using an independent-samples t-test in SPSS. Additional correlation analyses were done in SPSS to investigate if clinical or demographic variables account for any variance in BOLD- or CBF-CVR. This analysis included investigating the effect of EDSS, disease duration, and age.

3.4.5 Data Quality Control

Motion estimates for x-, y-, and z- translational motion and x-, y-, and z- rotational motion were calculated for all fMRI data runs using the ASL Data Processing Toolbox in SPM [101, 102]. As mentioned previously, data runs with more than 3 mm or 0.06 radians of motion (i.e. motion of more than the size of one functional voxel) were excluded from further analysis. This resulted in the exclusion of two task runs, one from a healthy control and one from an MS patient.

All raw data files were also assessed for the presence of other MRI artifacts. The most common artifact in the data was a ghosting artifact in the phase-encoding direction (**Figure 3.6**), which resulted in the exclusion of three healthy controls and three patients. Additionally, one patient was excluded due to a severe susceptibility artifact caused by a metal dental implant that impaired the ASL tagging.

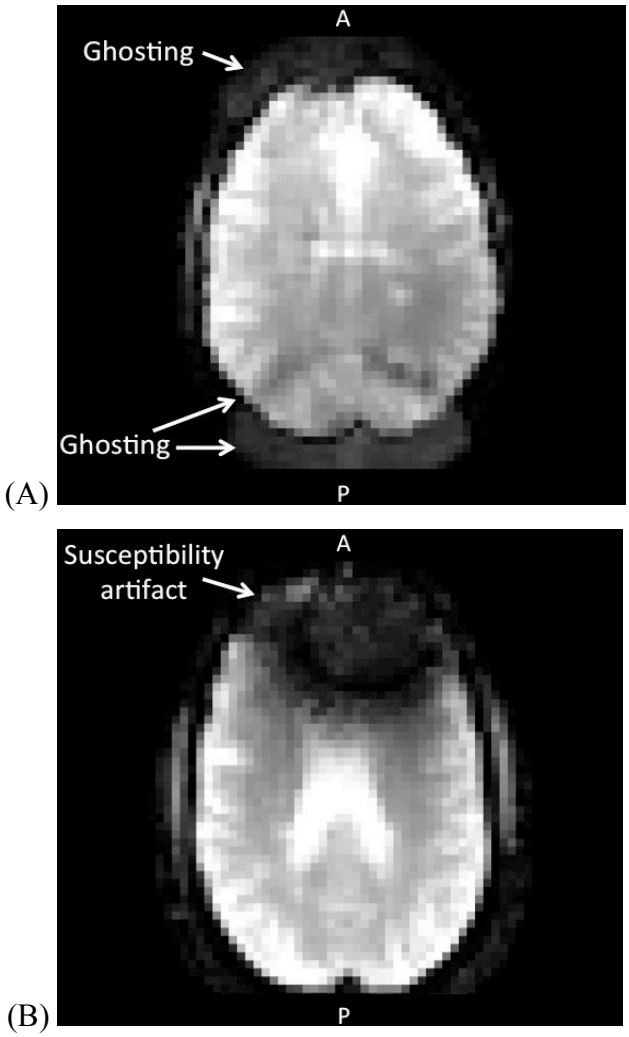

Figure 3.5: An axial slice of a ghosting artifact. P is posterior and A is anterior.

In MRI, SNR is the ratio of the amount of true signal, caused by actual anatomy, to the amount of background noise. SNR can also be measured across a time series (temporal SNR; tSNR) in order to determine SNR of fMRI sequences. As part of our data quality control, we calculated the tSNR for all fMRI data. Due to the low SNR of ASL data, the tSNR of the perfusion-subtracted data was the limiting factor for the data quality. All ROIs with tSNR lower than 1.0 for the perfusion-subtracted time series were excluded. This resulted in the exclusion of half of the ROIs of two MS patients. Furthermore ROIs with insufficient activation, defined as

having 10 or less activated voxels, were excluded from analysis, resulting in the exclusion of one MS patient, who had insufficient ROI activation in both task runs.

Lastly, analysis of behavioural data was completed to ensure participants were successfully performing the motor task. Specifically, task-performance was assessed by: 1) quantitative analysis of the percentage of time the participant pressed the correct buttons at the correct frequency, and 2) qualitative analysis of the video-camera footage to assess the presence of movement during the MI task. All included participants performed the physical finger-tapping (ME) task successfully over 95% of the time. Additionally, visual inspection of the video camera footage showed that all included participants successfully completed the MI task. Successful completion of the MI task was qualitative determined as containing no obvert voluntary hand movement.

Chapter Four: Results

All recruited participants gave consent on the day of their appointment and completed their study appointment successfully. Four healthy controls and four MS patients had high blood pressure (>120/80 mm Hg); the remaining participants had healthy blood pressure (<120/80 mm Hg). Additionally, hemoglobin and hematocrit levels were within normal in all participants, except one male MS patient, who had a hemoglobin level of 133 g/L (the normal hemoglobin level for males is 140-180 g/L). Demographic and clinical characteristics of the included participants are summarized in **Table 4.1**.

	Mean ± SD (range)		p-value
	MS group (n=12; 4M)	HC group (n=11; 2M)	(2-tailed)
Age (years)	51 ± 8 (37-61)	49 ± 9 (31-62)	.49
Hemoglobin (g/L)	143 ± 8 (133-158)	141 ± 11 (128-167)	.55
Hematocrit (L/L)	.44 ± .03 (.41-.49)	.43 ± .03 (.38-.51)	.29
T-25FW (seconds)	4.15 ± 0.66 (3.32-4.90)	3.90 ± 0.56 (3.41-5.04)	.36
9-HPT (seconds)			
Right hand	20.36 ± 4.15 (16.11-29.16)	18.69 ± 1.67 (15.67-20.95)	.23
Left hand	23.19 ± 6.45 (18.03-41.79)	20.00 ± 2.27 (16.96-22.9)	.14
SDMT	58 ± 10 (39-74)	65 ± 7 (53-78)	.06
MHI	4.66 ± 0.94 (2.22-5.56)	5.02 ± 0.84 (2.72-5.83)	.35
MFIS	29 ± 13 (10-53)	20 ± 18 (0-49)	.19
EDSS	2.3 ± 1.0 (1-4)	N/A	N/A
Disease duration (years)	16 ± 11 (3-38)	N/A	N/A
Time since relapse (years)	11 ± 10 (1-38)	N/A	N/A

Table 4.1: Summary of demographic and clinical characteristics of both groups.

Abbreviations: MS, multiple sclerosis; HC, healthy control; T-25FW, timed-25 foot walk; 9-HPT, 9 hole peg test; SDMT, symbol digit modality test; MHI, mental health inventory; MFIS, modified fatigue impact scale; EDSS, expanded disability status scale.

4.1 Flow-metabolism coupling, $CMRO_2$, BOLD, and CBF

4.1.1 Within-group voxel-wise Analysis of BOLD and CBF

Before the ROI analysis of flow-metabolism coupling, $CMRO_2$, BOLD, and CBF, between- and within-group voxel-wise analyses of ΔBOLD and ΔCBF were completed to analyze the effect of task (ME versus MI), in order to determine if MI can be used to investigate our fMRI measures, irrespective of the patient's hand motor function.

In the healthy control (HC) group, a voxel-wise repeated-measures ANOVA, conducted in FAST [115], showed that MI resulted in activation of the motor network, in similar areas activated by ME. This finding was consistent for both BOLD (**Figure 4.1**) and CBF (**Figure 4.2**) measures.

Furthermore, ME and MI resulted in activation of similar areas of the motor network in the MS group as well. This finding was consistent in both the voxel-wise ΔBOLD (**Figure 4.3**) and voxel-wise ΔCBF (**Figure 4.4**) analyses.

Between-group analysis of voxel-wise ΔBOLD and ΔCBF in ME and MI showed that similar motor network areas are activated in both groups for the ME task and the MI task; however, some differences were found between the two groups. F-tests were conducted to investigate areas where the HC group had higher activation and areas where the MS group had higher activation. The results of the ΔBOLD voxel-wise analysis are summarized in **Figure 4.5** and the ΔCBF voxel-wise results are summarized in **Figure 4.6**.

(A)

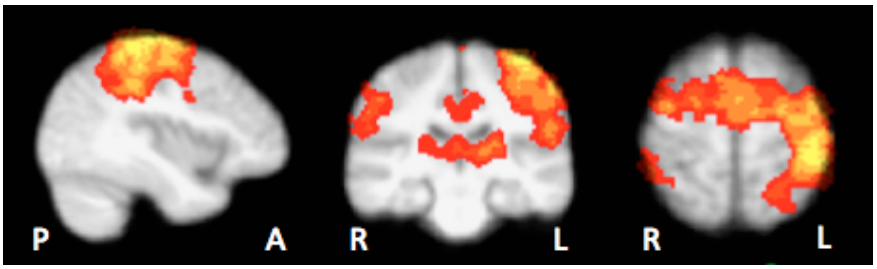

(B)

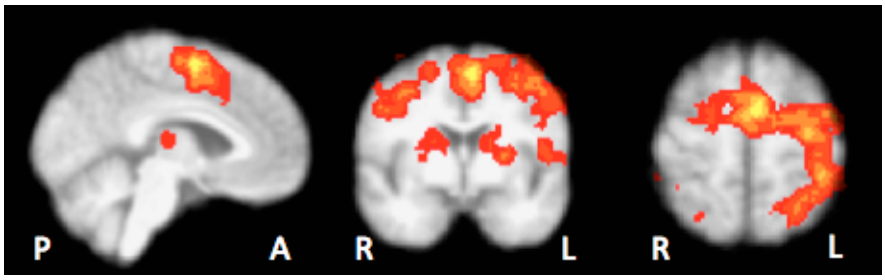

(C)

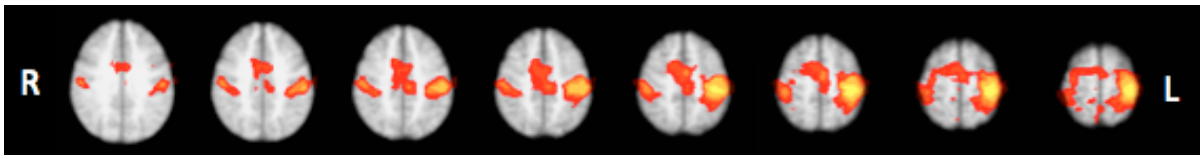

(D)

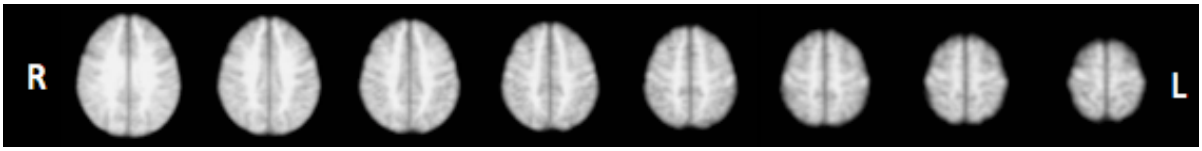

Figure 4.1: ΔBOLD within-group comparison of ME- versus MI-induced brain activation in the healthy control group.

The sagittal (left), coronal (middle) and axial (right) views of the peak BOLD activation cluster for the ME task and MI task in the HC group are shown in (A) and (B), respectively. BOLD ME-activation (A) is predominantly in the contralateral premotor cortex, and also in the contralateral primary motor cortex, contralateral primary somatosensory cortex, ipsilateral premotor cortex, ipsilateral primary somatosensory cortex, and bilateral corticospinal tract. BOLD MI-activation in (B) is predominantly in the contralateral and medial premotor cortex, and also in the contralateral primary motor cortex, contralateral primary somatosensory cortex, ipsilateral premotor cortex, ipsilateral primary somatosensory cortex, and bilateral corticospinal tract. (C) shows the HC group contrast map for areas where BOLD ME-activation is greater than BOLD MI-activation; ME appears to cause greater BOLD activation predominantly in the contralateral primary somatosensory cortex, and also causes slightly greater BOLD activation in the contralateral premotor cortex, contralateral primary motor cortex, contralateral corticospinal tract, and the ipsilateral primary somatosensory cortex. (D) shows the HC group contrast map for areas where BOLD MI-activation is greater than BOLD ME-activation; no areas were found to have significantly more BOLD activation in MI versus ME. These maps (C and D) are z-thresholded at 2.3 and cluster corrected at $p = .05$). All images are in radiological view; L, left; R, right.

(A)
(B)
(C)
(D)

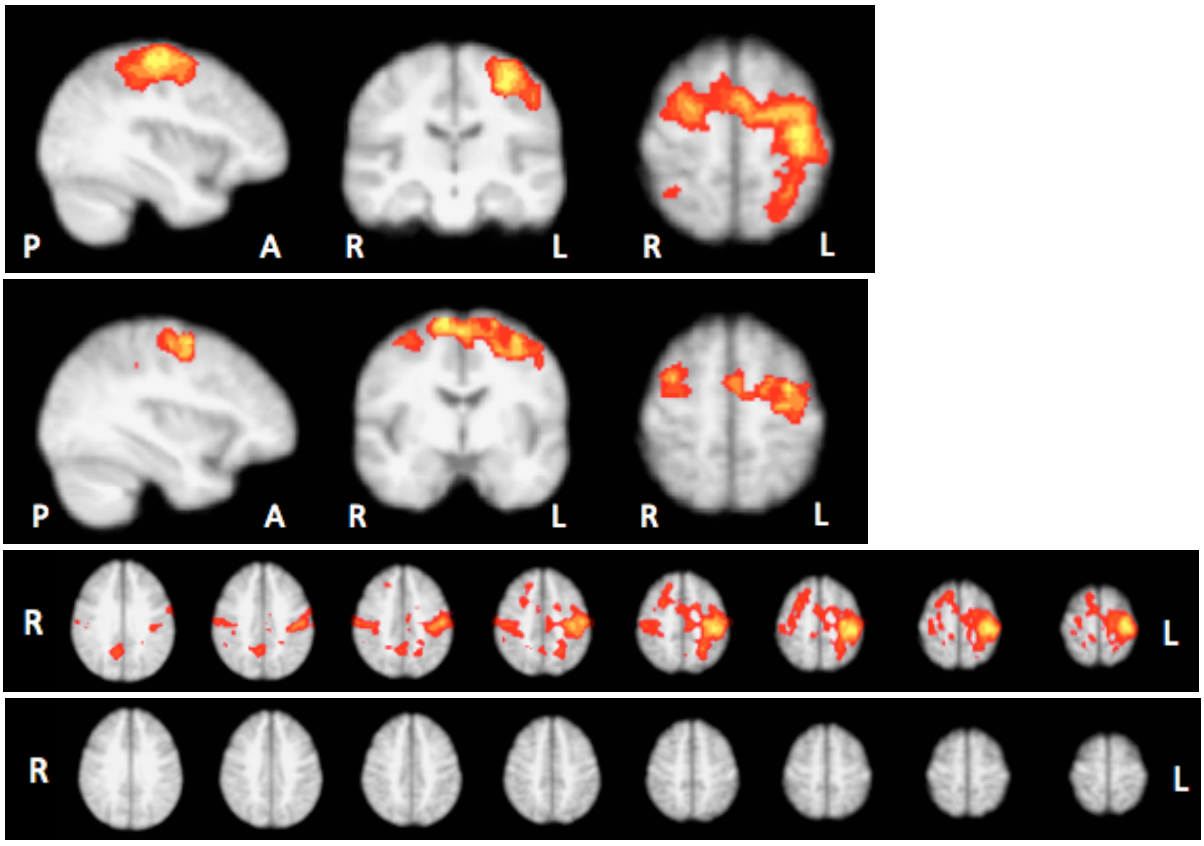

Figure 4.2: ΔCBF within-group comparison of ME- versus MI-induced brain activation in the healthy control group.

The sagittal (left), coronal (middle) and axial (right) views of the CBF activation cluster for the ME task and MI task in the HC group are shown in (A) and (B), respectively. CBF ME-activation (A) is predominantly in the contralateral premotor cortex, and also in the contralateral primary motor cortex, contralateral primary somatosensory cortex, and ipsilateral premotor cortex. CBF MI-activation in (B) is predominantly in the contralateral and ipsilateral premotor cortices. (C) shows the HC group contrast map for areas where CBF ME-activation is greater than CBF MI-activation; ME appears to cause greater CBF activation predominantly in the contralateral primary motor and primary somatosensory cortices, and also causes greater CBF activation in the contralateral premotor cortex and the ipsilateral primary somatosensory cortex. (D) shows the HC group contrast map for areas where CBF MI-activation is greater than CBF ME-activation; no areas were found to have significantly more CBF activation in MI versus ME. These maps (C and D) are z-thresholded at 2.3 and cluster corrected at $p = .05$). All images are in radiological view; L, left; R, right.

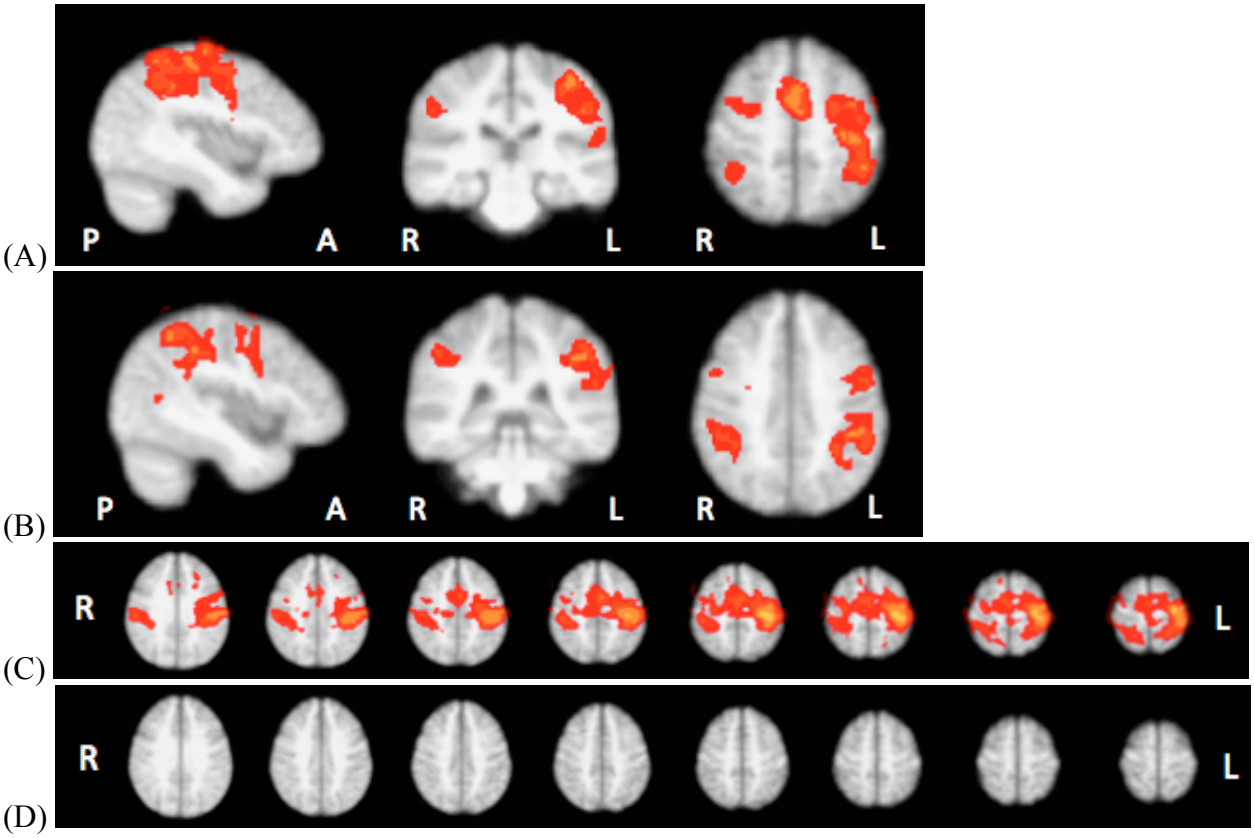

Figure 4.3: ΔBOLD within-group comparison of ME- versus MI-induced brain activation in the MS group.

The sagittal (left), coronal (middle) and axial (right) views of the BOLD activation cluster for the ME task and MI task in the MS group are shown in (A) and (B), respectively. BOLD ME-activation (A) is predominantly in the medial and contralateral premotor cortex, contralateral primary motor cortex, and contralateral primary somatosensory cortex, and also in the ipsilateral premotor cortex and ipsilateral primary somatosensory cortex. BOLD MI-activation in (B) is predominantly in the medial and contralateral premotor cortex and contralateral primary somatosensory cortex, and also in the contralateral primary motor cortex, ipsilateral premotor cortex, and ipsilateral somatosensory cortex. (C) shows the MS group contrast map for areas where BOLD ME-activation is greater than BOLD MI-activation; ME appears to cause greater BOLD activation predominantly in the contralateral premotor cortex, contralateral primary motor cortex, contralateral primary somatosensory cortex, and also causes slightly greater BOLD activation in the ipsilateral premotor cortex, ipsilateral primary motor cortex, ipsilateral primary somatosensory cortex, and bilateral corticospinal tract. (D) shows the MS group contrast map for areas where BOLD MI-activation is greater than BOLD ME-activation; no areas were found to have significantly more BOLD activation in MI versus ME. These maps (C and D) are z-thresholded at 2.3 and cluster corrected at p = .05). All images are in radiological view; L, left; R, right.

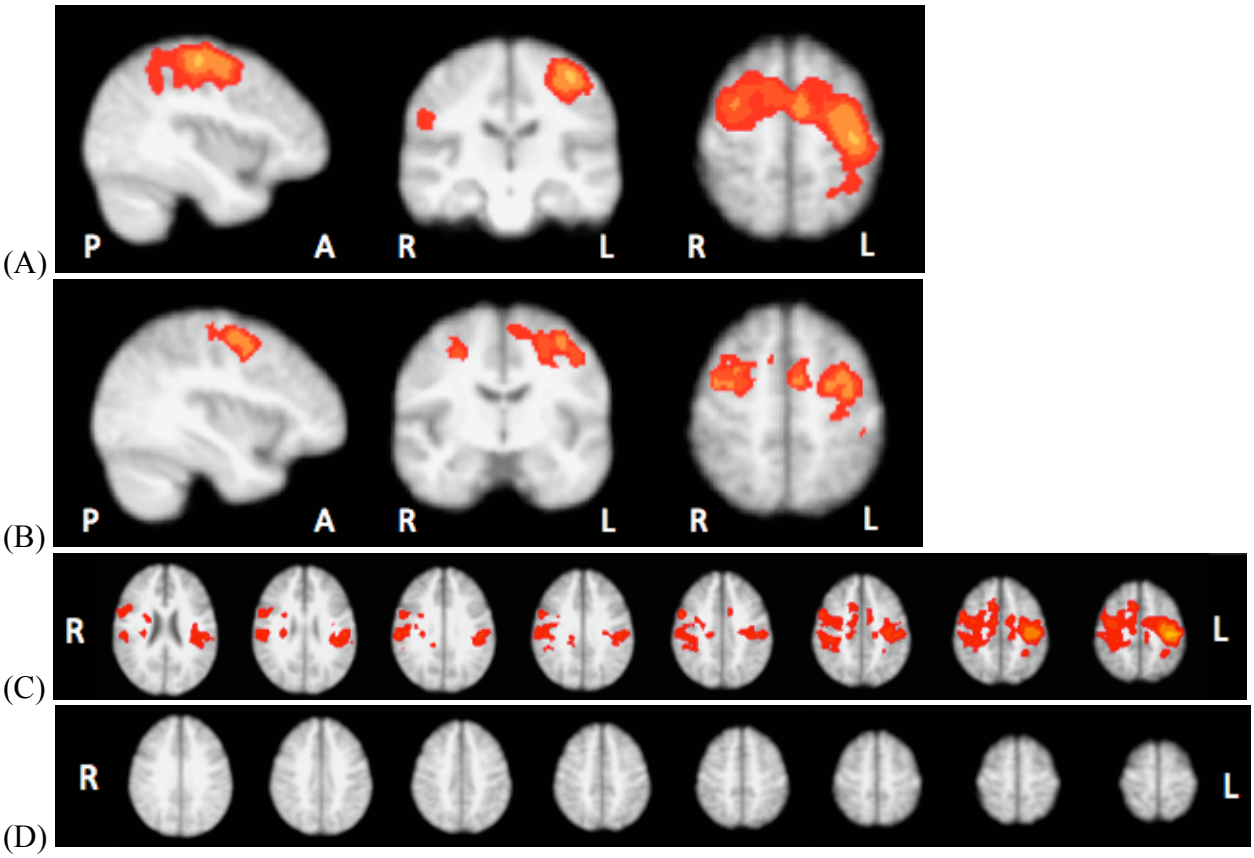

Figure 4.4: ΔCBF within-group comparison of ME- versus MI-induced brain activation in the MS group.

The sagittal (left), coronal (middle) and axial (right) views of the CBF activation cluster for the ME task and MI task in the MS group are shown in (A) and (B), respectively. CBF ME-activation (A) is predominantly in the contralateral premotor cortex, ipsilateral premotor cortex, contralateral primary motor cortex, contralateral primary somatosensory cortex, and also in the ipsilateral somatosensory cortex. CBF MI-activation in (B) is predominantly in the contralateral and ipsilateral premotor cortices, and also in the contralateral primary motor cortex. (C) shows the MS group contrast map for areas where CBF ME-activation is greater than CBF MI-activation; ME appears to cause greater CBF activation predominantly in the contralateral premotor cortex, contralateral primary motor cortex, contralateral primary somatosensory cortex, and also causes greater CBF activation in the ipsilateral premotor cortex, ipsilateral primary motor cortex, and ipsilateral somatosensory cortex. (D) shows the MS group contrast map for areas where CBF MI-activation is greater than CBF ME-activation; no areas were found to have significantly more CBF activation in MI versus ME. These maps (C and D) are z-thresholded at 2.3 and cluster corrected at $p = .05$). All images are in radiological view; L, left; R, right.

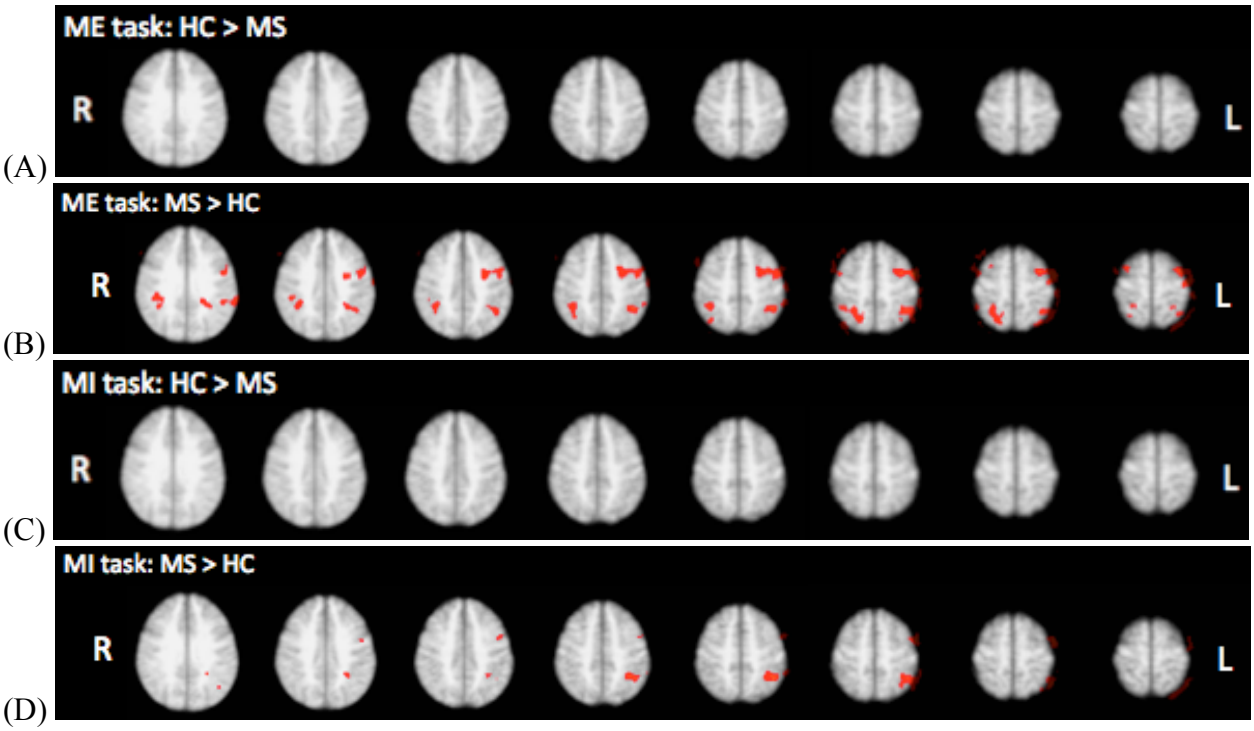

Figure 4.5: ΔBOLD voxel-wise between-group analysis (z = 3, cluster p-threshold < .05).

(A) shows no significantly higher ME-induced activation in the HC group compared to the MS group and (B) shows higher ME-induced BOLD activation in the MS group in the contralateral premotor cortex and bilaterally in the superior and inferior parietal lobe, specifically in the anterior intra-parietal sulcus. For the MI-task, no areas were significantly more activated in the HC group (C); however, the MS group had higher MI-induced BOLD activation in the superior and inferior parietal lobe, specifically in the anterior intra-parietal sulcus (D).

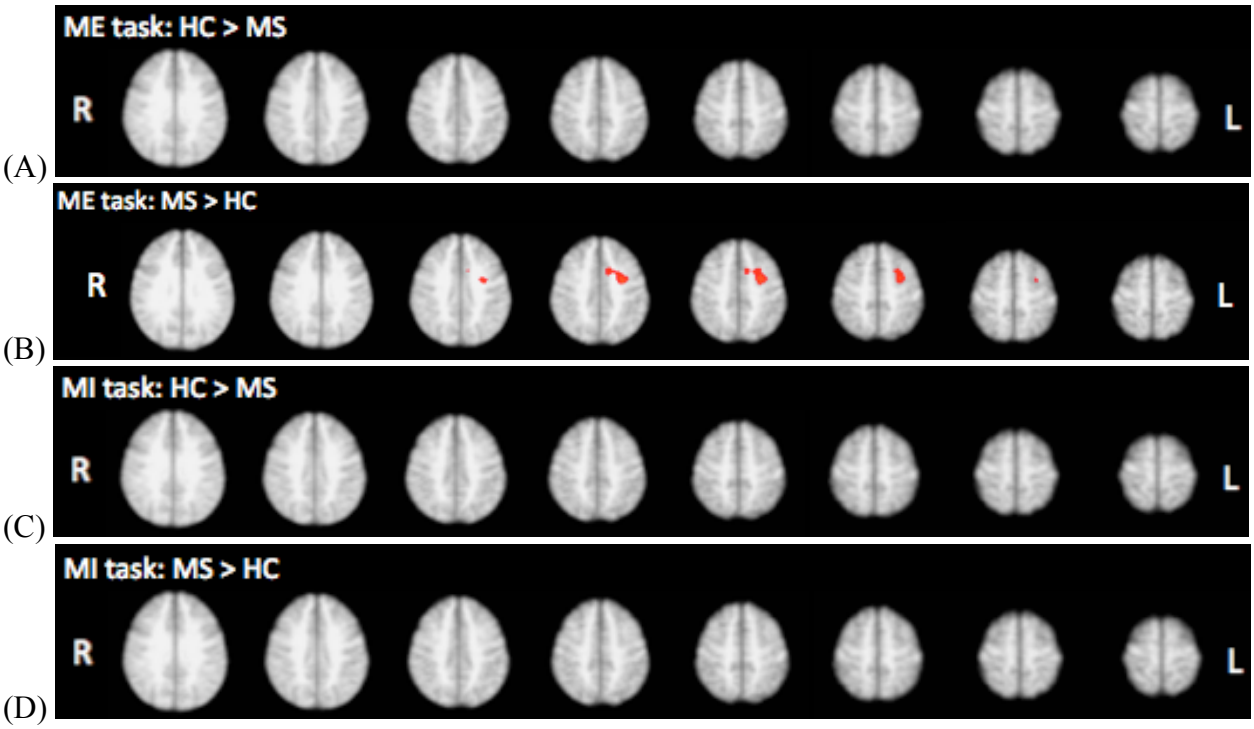

Figure 4.6: ΔCBF voxel-wise between-group analysis (z = 3, cluster p-threshold < .05). (A) shows no significantly higher ME-induced CBF activation in the HC group compared to the MS group; however, (B) shows the MS group had slightly higher CBF activation in the left cerebral white matter, as compared with the MS group. The CBF voxel-wise analysis of the MI task found no significant differences between groups in either direction (C and D).

4.1.2 ROI analysis of flow-metabolism coupling, $CMRO_2$, BOLD, and CBF

Functional measures of cerebral physiology in the three ROIs were analyzed using two-way repeated measures linear mixed effects ANOVA in SPSS. For all measures, we were primarily interested in the main effect of group; however, the main effect of task was also investigated. For all analyses of each measure and in each ROI, no interaction effect between group and task was found; therefore, the simple main effects of group and task were not investigated. Four measures, BOLD, CBF, $CMRO_2$, and flow-metabolism ratio, were analyzed in three different ROIs; therefore, a Bonferroni correction was applied to correct for 12 multiple comparisons, yielding a α-threshold of 0.0042. All group effects are summarized in **Table 4.2**.

BOLD Results

After correcting for multiple comparisons, BOLD percent signal change (psc) in the premotor cortex was not significantly different between groups ($p = .01$); however, it was significantly different between the two task types ($p = .003$), where the ME task had significantly higher BOLD psc (.83%) than the MI task (.71%) across both groups. BOLD psc in the primary motor cortex was found to be not significantly different between groups ($p = .708$); however, an effect of task was found ($p = .001$) where ME had a higher BOLD psc than MI in the primary motor cortex. BOLD psc in the primary somatosensory cortex was found to be not significantly different between groups ($p = .632$); however, there was a significant effect of task ($p = .0002$) where ME had a higher BOLD psc than MI in the primary somatosensory cortex.

CBF Results

CBF percent signal change (psc) in the premotor cortex was significantly different between groups ($p = .006$) and task type ($p = .01$); however, these two measures lost their significance after multiple comparisons were corrected for. Baseline CBF in the premotor cortex was not significantly different between groups ($p = .244$). CBF psc in the primary motor cortex was found to be significantly different for groups ($p = .0008$) and task type ($p = .000001$). Additionally, baseline CBF in the primary motor cortex was significantly different between groups ($p < .0001$). CBF psc in the primary somatosensory cortex was found to be significantly different between groups ($p = .0002$), and an effect of task was also found ($p = .00002$), with ME CBF psc = 27.7% and MI CBF psc = 19.1%. Baseline CBF in the primary somatosensory cortex was significantly different between groups ($p = .0036$).

$CMRO_2$ Results

No main effect of group ($p = .173$) or task type ($p = .375$) was found for $CMRO_2$ psc in the premotor cortex; the mean $CMRO_2$ psc for the ME task was 10.9% versus 9.6% for the MI task. In the primary motor cortex, no effect of group was found ($p = .078$); however, $CMRO_2$ psc was significantly different ($p = .02$) in ME (10.0%) versus MI (7.4%). No main effect of group ($p = .069$) or task type ($p = .103$) was found in the primary somatosensory cortex for $CMRO_2$ psc.

Flow-metabolism Ratio Results

No main effect of group ($p = .095$) or task type ($p = .768$) was found for the flow-metabolism ratio in the premotor cortex. No main effect of group ($p = .752$) or task type ($p = .890$) was found for the flow-metabolism ratio in the primary motor cortex. No main effect of group ($p = .108$) or task type ($p = .452$) was found for the flow-metabolism ratio in the primary somatosensory cortex. Scatterplots comparing the relationship between CBF psc and $CMRO_2$ psc in both groups are shown in **Figure 4.7**.

(A)

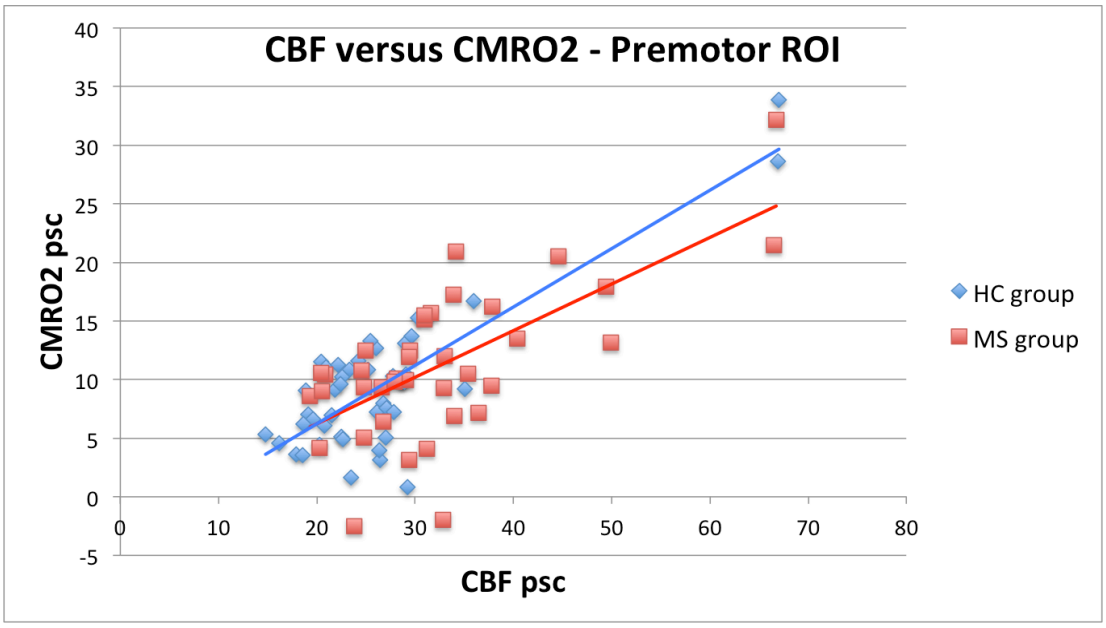
CBF versus CMRO2 - Premotor ROI
CMRO2 psc
CBF psc
HC group
MS group
40
35
30
25
20
15
10
5
0
-5
0
10
20
30
40
50
60
70
80

(B)

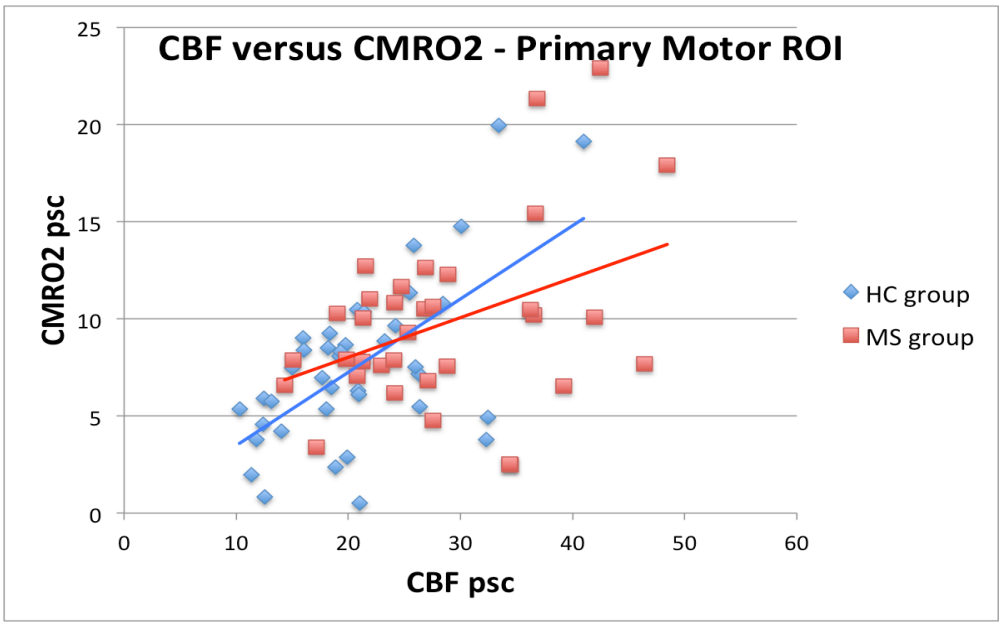
CBF versus CMRO2 - Primary Motor ROI
CMRO2 psc
CBF psc
HC group
MS group
25
20
15
10
5
0
0
10
20
30
40
50
60

(C)

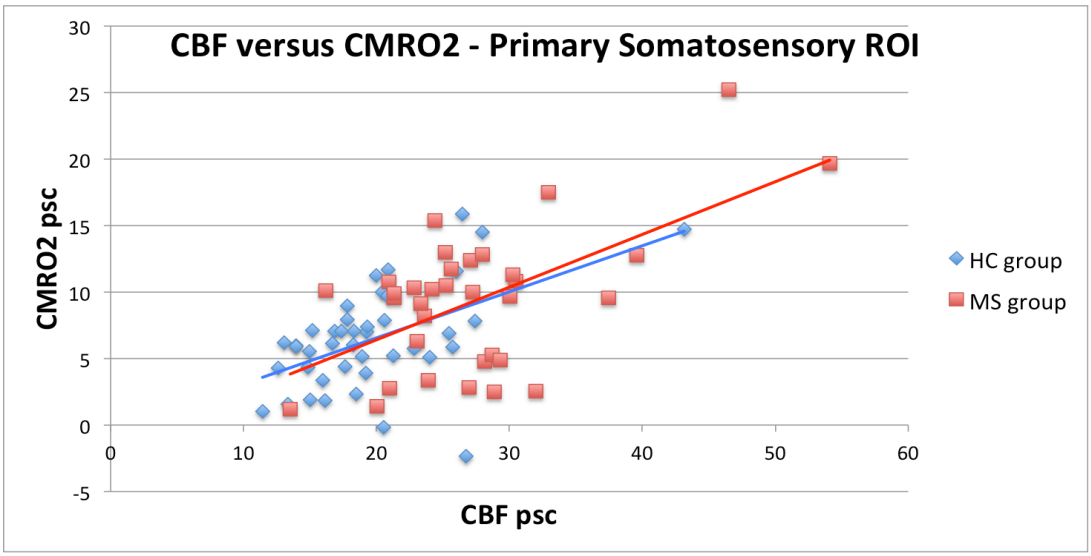

Figure 4.7: Scatterplots comparing $CMRO_2$ psc versus CBF psc between the two groups.

The relationship between CBF and $CMRO_2$ was not significantly different between groups in the premotor cortex (A), the primary motor cortex (B), or the primary somatosensory cortex (C).

	Group Mean (SD)		f-test	
Measure	HC group	MS group	f-statistic	p-value
BOLD psc				
Premotor ROI	.72 (.15)	.83(.25)	7.03	.010*
Primary motor ROI	.56 (.24)	.59(.18)	.142	.708
Primary somatosensory ROI	.75 (.29)	.75(.28)	.231	.632
CBF psc				
Premotor ROI	26.2 (10.1)	32.7 (10.9)	8.04	.006*
Primary motor ROI	21.8 (9.0)	28.4 (8.9)	12.47	.0008**
Primary somatosensory ROI	20.9 (9.6)	27.4 (7.9)	15.91	.0002**
$CMRO_2$ psc				
Premotor ROI	9.3 (6.1)	11.3 (6.5)	1.90	.173
Primary motor ROI	8.2 (5.6)	9.7 (4.6)	3.21	.078
Primary somatosensory ROI	7.2 (6.3)	9.4 (5.3)	3.43	.069
Flow-metabolism ratio				
Premotor ROI	4.2 (5.3)	2.3 (4.1)	2.92	.095
Primary motor ROI	4.3 (6.1)	3.7 (2.8)	.101	.752
Primary somatosensory ROI	3.2 (3.2)	4.4 (3.5)	1.26	.267

Table 4.2: Summary of group main effects for task-induced fMRI measures.

* p-values are significant at the uncorrected p-threshold but loose significance at the corrected p-threshold; ** p-values are significant at the corrected p-threshold.

4.2 Cerebrovascular Reactivity

After the previously discussed data exclusion criteria were applied, analysis of BOLD-CVR and CBF-CVR was performed on the data from 12 MS patients and 11 healthy controls. The mean baseline $ETCO_2$ was 31.3 (1.6) mm Hg in the HC group and 33.6 (4.1) mm Hg in the MS group. The mean change in $ETCO_2$ was 9.91 (1.30) mm Hg in the HC group and 9.08 (2.02) mm Hg in the MS group. Baseline $ETCO_2$ and hypercapnia-induced change in ETCO2 were not significantly different between groups, where $p = .10$ and $p = .26$, respectively.

Voxel-wise analysis of the hypercapnia-induced BOLD response showed no significant differences between the two groups (**Figure 4.8**).

Voxel-wise analysis of the hypercapnia-induced CBF response also showed no significant between-group differences (**Figure 4.9**).

Independent samples t-test analyses were completed to compare the computed values of BOLD-CVR and CBF-CVR in the subject-specific GM ROIs. The mean GM BOLD-CVR was .255 (.093) in the control group and .275 (.103) in the MS group, measured in units of BOLD percent signal change per mm Hg $ETCO_2$; no significant GM BOLD-CVR between-group difference was found ($t = .500$; $p = .622$) (**Figure 4.10A**). The mean GM CBF-CVR was 3.90 (1.73) in the control group and 3.61 (1.08) in the MS group, measured in units of CBF percent signal change per mm Hg $ETCO_2$; in concordance with the GM BOLD-CVR findings, no significant GM CBF-CVR between-group difference was found either ($t = .492$; $p = .628$) (**Figure 4.10B**). These results, as well as the group means of global GM normocapnia and hypercapnia BOLD, CBF, and $ETCO_2$ values, are summarized in **Table 4.3**.

An independent samples t-test revealed that there was a significant difference in grey matter baseline CBF between the two groups ($p = .023$), with the MS group having a lower mean baseline CBF value (41.42 mL/100 g/min) compared to the HC group (50.41 mL/100 g/min).

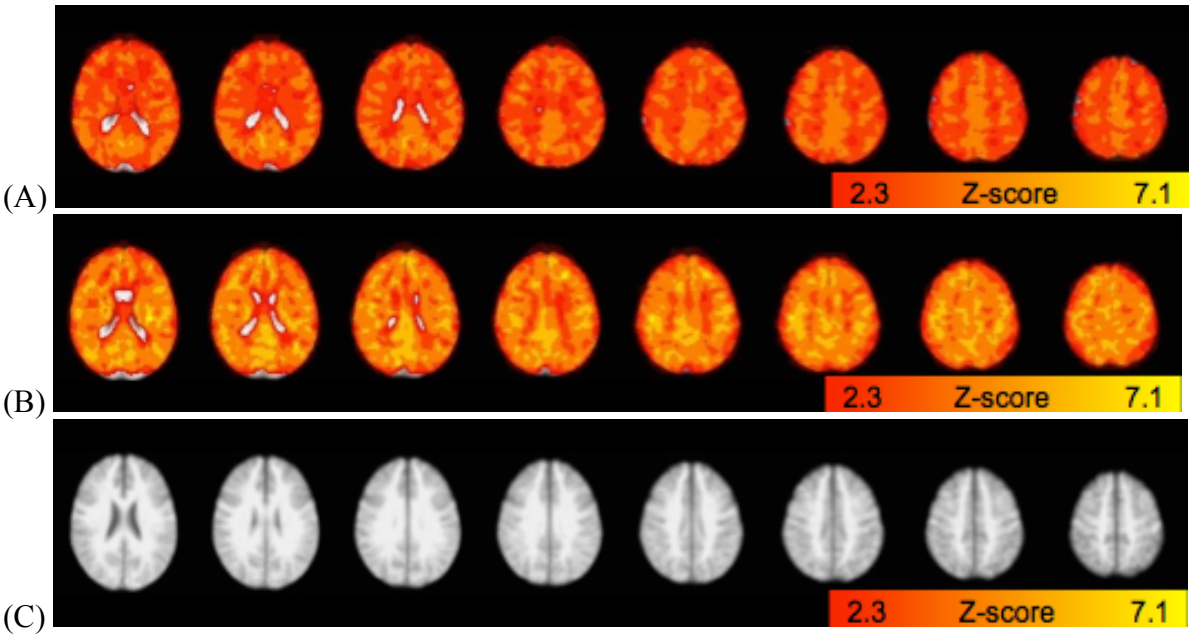

Figure 4.8: BOLD cerebrovascular reactivity (BOLD-CVR) z-statistic maps.

(A) shows the control group map and (B) shows the MS group map for areas where hypercapnia-BOLD > normocapnia BOLD. (C) shows there were no significant BOLD-CVR differences between the two groups.

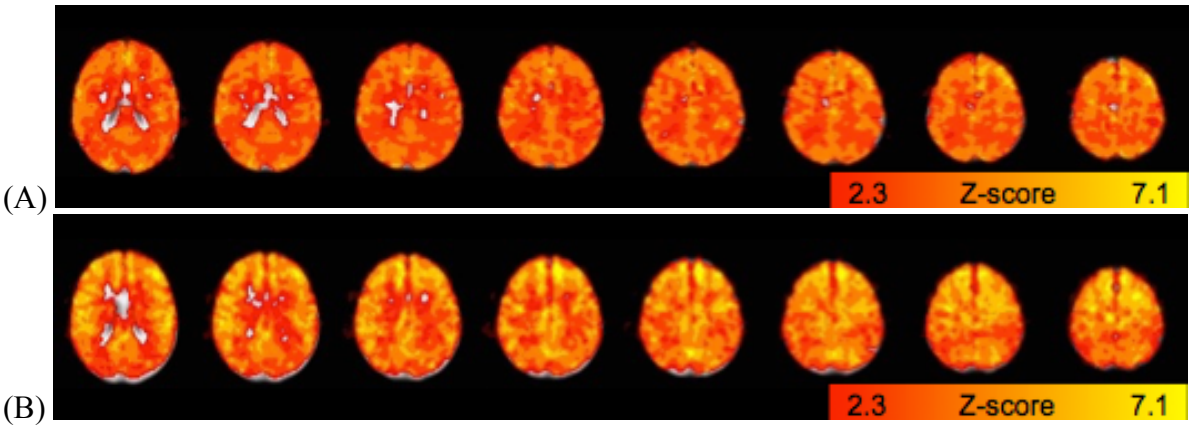

(C) 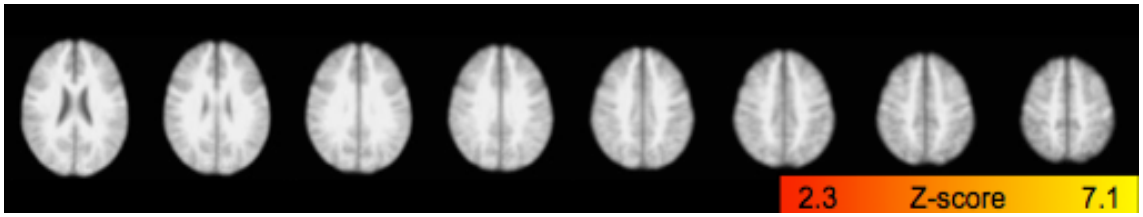

Figure 4.9: CBF cerebrovascular reactivity (CBF-CVR) z-statistic maps.

(A) shows the control group map and (B) shows the MS group map for areas where hypercapnia-CBF > normocapnia CBF. (C) shows there were no significant CBF-CVR differences between the two groups.

(A) 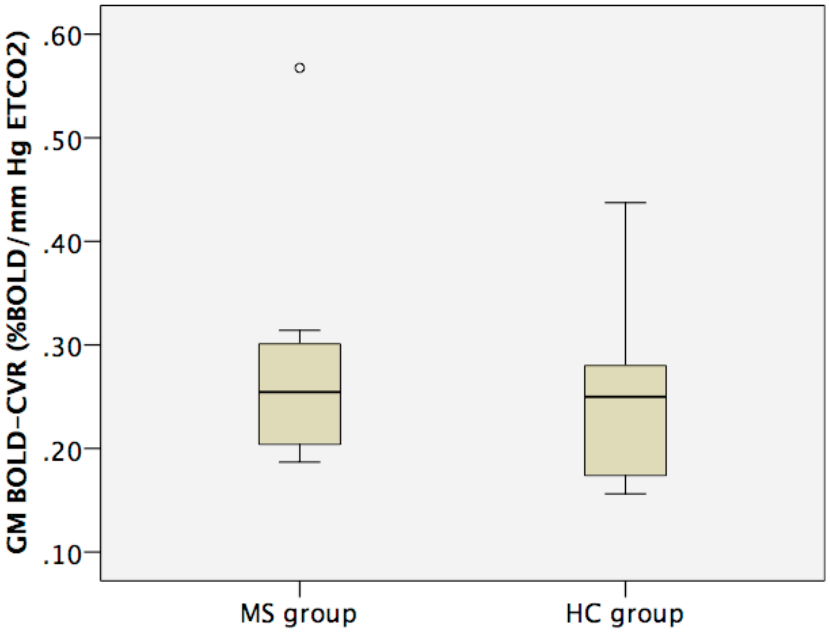

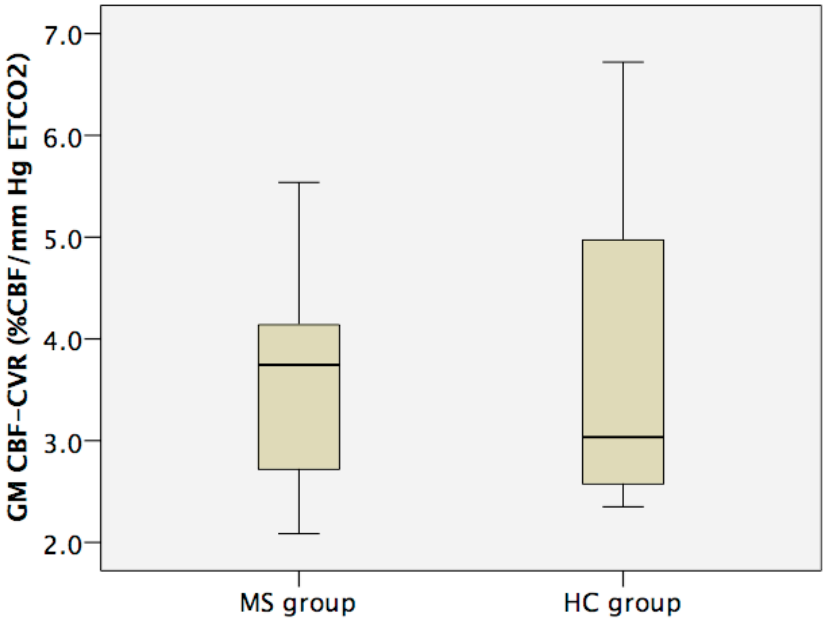

(B)

Figure 4.10: Box-plot group comparisons of GM BOLD-CVR and GM CBF-CVR.

GM BOLD-CVR (A) is calculated as the percent signal change of normocapnia to hypercapnia BOLD divided by the change in end-tidal partial pressure of CO_2. Similarly, GM CBF-CVR (B) is calculated as the percent signal change of normocapnia to hypercapnia CBF divided by the change in end-tidal partial pressure of CO_2.

	Mean (SD)		Independent t-test	
Measure	Control group	MS group	|t-statistic|	p-value
Difference				
BOLD psc	2.46 (.750)	2.33 (.375)	.519	.609
CBF psc	37.3 (13.5)	31.5 (8.11)	1.25	.224
$ETCO_2$ mm Hg	9.91 (1.30)	9.08 (2.02)	1.15	.262
CVR				
BOLD-CVR (%BOLD/mm Hg $ETCO_2$)	.255 (.093)	.275 (.103)	.500	.622
CBF-CVR (%CBF/mm Hg $ETCO_2$)	3.90 (1.73)	3.61 (1.08)	.492	.628

Table 4.3: Summary of BOLD, CBF, and CVR results for the hypercapnia challenge.

All BOLD, CBF, and CVR values are global averages calculated across all GM voxels. The difference in $ETCO_2$ was calculated as the difference, in units of mm HG, between $ETCO_{2,hypercapnia}$ and $ETCO_{2,normocapnia}$.

As expected, the two measures of CVR, BOLD-CVR and CBF-CVR, were significantly correlated in the HC group (Pearson's r = .795, p = .003). BOLD-CVR and CBF-CVR were also significantly correlated in the MS group (Pearson's r = .627, p = .029), although the correlation was not as strong as the HC group.

There was no significant correlation found in the MS group between CBF-CVR and EDSS (Spearman's rho = .452, uncorrected-p = .140); however, there was a significant correlation found between BOLD-CVR and EDSS (Spearman's rho = .580, uncorrected-p = .048). The significant correlation between BOLD-CVR and EDSS in the patient group lost its significance after the Bonferroni-adjusted alpha-threshold of .008 (correcting for six correlation tests) was applied. No significant correlation was found between disease duration and BOLD- or CBF-CVR (Pearson's r = -.47, uncorrected-p = .12; Pearson's r = -.12, uncorrected-p = .71, respectively) in the MS group. Additionally, for all participants, no significant correlation was found between BOLD-CVR and age (Pearson's r = .18, uncorrected-p = .41) or between CBF-CVR and age (Pearson's r = .16, uncorrected-p = .46).

Chapter Five: Discussion

Before discussing the results of this research, two data quality issues should be addressed: phase-encoding ghosting artifacts and low tSNR. Together, these two issues, which often presented as mutually inclusive confounds, resulted in the exclusion of three out of 15 healthy controls and three out of 16 MS patients. The occurrence of Nyquist ghosting artifacts in our fMRI data is likely due to the EPI sequence used to collect all fMRI data. EPI sequences are susceptible to these ghosting artifacts because of the way images are collected, whereby adjacent phase-encoding lines are acquired in alternating directions. The even numbered echoes must be time-reversed to match the direction of the odd numbered echoes before image reconstruction [125]. Small temporal fluctuations, or phase shifts, in this time-reverse matching produce the observed Nyquist ghosting. These phase shifts can be caused by poor shimming, gradient coil heating, reconstruction errors, and eddy currents, which can cause B_0 distortions [126]. The specific EPI pulse sequence used in this thesis was not equipped with a more advanced phase-correction scheme to mitigate these Nyquist effects [125]. The visual severity of these EPI Nyquist effects become even larger when employing image acceleration techniques, such as SENSitivity Encoding [127] or ASSET [128], which was used here. Similarly, periodic movement during EPI data acquisition, such as cardiac or respiratory motion, can introduce additional phase shifts that introduce more ghosting artifacts [126]. The majority of these physiological ghosting artifacts occurred in the hypercapnia challenge gas run, which could be caused by increased respiratory motion in response to slight resistance in the breathing circuit or deeper breathing by the subjects.

As discussed in Section 3.4.5, all fMRI data with perfusion-subtraction tSNR values less than 1.0 were excluded. Low tSNR appeared to be mainly associated with the presence of the

aforementioned ghosting artifacts. Low tSNR on its own only resulted in the exclusion of data from specific ROIs of two patients and one healthy control, but did not result in full exclusion of any participants. Visual inspection of motion correction parameters showed that most of these excluded ROIs were from task runs with periodic motion.

The high occurrence of ghosting and low tSNR in the data presented in this thesis is a large limitation, as together these resulted in the exclusion of ~20% of the data, in addition to another ~5% of data that was excluded for other singleton reasons. After data quality exclusion, the study sample consisted of 12 MS patients and 11 healthy controls. All results presented in this thesis are from included data only.

Comparison of mean values of demographic and clinical characteristics revealed that the two groups were comparable across all domains, other than patient specific domains, such as EDSS. Specifically, the two groups did not significantly differ in age, T-25FW scores, 9-HPT scores, SMDT scores, MHI scores, MFIS scores, or hemoglobin/hematocrit values. These similarities between groups reduces the risk of participant-specific or non-disease group-related confounds having an effect on the data.

5.1 Task-Related fMRI measures of cerebral physiology

5.1.1 Voxel-wise analysis of BOLD and CBF – comparing ME versus MI

In this research, we first investigated within- and between-group effects of ME versus MI task-induced activation. The motivation behind this investigation was to determine whether MI, which is not dependent on physical motor ability, can be used to access and activate the motor network in MS patients, who often have motor disabilities. Although ME and MI are both motor tasks, there have been doubts in the past about whether they both activate similar cortical areas.

Specifically, it has been suggested that bilateral MI will not activate cortical regions responsible for execution of movement, but rather will only activate areas involved in motor planning, such as the left posterior parietal and left motor areas, which have been shown to be responsible for motor planning of both hands [129-131]. Execution of movement recruits these motor planning areas as well; however, bilateral motor areas, including the premotor and primary motor cortices, are also recruited for motor execution [132, 133]. Previous studies in healthy controls have shown that there is congruent activation of the motor system for ME and MI tasks [4, 134, 135]; however, this congruency of activation has not been investigated in MS patients.

In agreement with these previous studies [4, 134, 135], our analysis of BOLD and CBF measures showed that MI successfully activated similar areas as ME in the HC group. In the HC group, both tasks caused BOLD-activation in the contralateral premotor cortex, contralateral primary motor cortex, contralateral somatosensory cortex, ipsilateral premotor cortex, ipsilateral primary somatosensory cortex, and bilateral corticospinal tract. The ME task caused greater BOLD-activation in the majority of these regions, but they were also activated by the MI task. Additionally, both tasks caused CBF-activation of premotor, primary motor, and somatosensory cortical areas; however, ME caused greater CBF-activation in the contralateral primary motor cortex, contralateral primary somatosensory cortex, contralateral premotor cortex, and ipsilateral primary somatosensory cortex. Overall, in healthy controls, although ME causes higher BOLD and CBF activation, MI activates the main motor regions that are activated by ME; this finding is in agreement with previous studies [4, 134, 135]. (**Figures 4.1 and 4.2**)

Of particular interest to this study was whether these similarities between ME and MI activation extend to MS patients, and our findings suggest that they do. In the MS group, ME caused both BOLD and CBF activation in the contralateral premotor cortex, contralateral

primary motor cortex, contralateral primary somatosensory cortex, and also ipsilateral premotor and somatosensory cortices. MI caused similar BOLD and CBF activation patterns in these patients; however the MI-induced activation was slightly lower than ME-induced activation in most of these regions. (**Figures 4.3 and 4.4**)

In addition to these within-group analyses on the effect of task, between-group analyses were conducted to investigate the effect of group on ME versus MI activation. Overall, minimal between-group differences were found. For BOLD and CBF, the HC group did not have any regions of significantly higher activation than the MS group for either of the two tasks. The main voxel-wise between-group difference was that the MS group had greater BOLD-activation for both tasks in the parietal lobe, specifically in the anterior intra-parietal sulcus (**Figure 4.5**). The MS group also had greater CBF-activation in a region of the left cerebral white matter (**Figure 4.6**). To summarize, ME and MI appear to similarly activate the motor network in both groups, suggesting that the level of disability seen in this group of RRMS patients does not significantly disrupt the motor imagery network. Additionally, the main group and task differences are with respect to the magnitude of activation rather than differences in the spatial extent of the activation.

Taken together, these within- and between-group findings suggest that MI can be used to access and activate the motor network in MS patients. Therefore, for the present study as well as future fMRI MS studies, MI can be used to investigate fMRI measures irrespective of the patient's physical hand motor function. Furthermore, these results provide the rationale for future investigations on the applicability of MI tasks in MS, for example, the ability for motor imagery to be efficacious for maintaining or improving motor function in MS, similar to what has been studied in other neurological conditions, such as stroke [136, 137].

5.1.2 ROI analysis of flow-metabolism, $CMRO_2$, BOLD, and CBF

After validating the use of MI as an additional task in our study, we investigated a number of physiological fMRI measures in MS patients compared to healthy controls. In addition to investigating the conventional fMRI measure of BOLD, we explored and quantified physiological processes that underlie the BOLD response. We looked at these physiological responses to a typical ME task, and also to a MI task, which was used to control for physical hand motor function. fMRI measures were analyzed in three functionally defined ROIs: the left premotor cortex, the left primary motor cortex, and the left primary somatosensory cortex (shown in **Figure 3.5**). These cortical regions have all been shown, in this study and previous studies, to play an essential role in performing motor tasks. ROIs were chosen to be unilateral (left only) because the motor task was a unilateral right-hand task. The ipsilateral motor network does show activation during a unilateral motor task, as highlighted in the previous discussion on ME versus MI; however, the primary goal of this study was to explore the physiology of the BOLD response in MS patients, therefore, analysis of both hemispheres would be redundant.

BOLD Results

Our BOLD ROI analysis revealed a significant effect of task, where the ME task had higher BOLD psc than the MI task in all three ROIs. This finding was to be expected as it is consistent with the finding from the previous voxel-wise analysis of ME and MI, whereby the extent and magnitude of MI-induced BOLD activation appear to be attenuated compared to ME-induced activation (**Figures 4.1 and 4.2**).

The BOLD ROI analysis did not find any significant effects of group at either level of task, suggesting that the BOLD response in the motor network may be unaltered in this group of MS patients. This finding is inconsistent with the most commonly reported BOLD finding in MS patients, which is that MS patients demonstrate increased BOLD activation compared to healthy controls [50, 60, 138-140]. The reason for this discrepancy could be due to differences in the patient inclusion/exclusion criteria and clinical characteristics, specifically, our MS patients were all of the relapsing remitting subtype, and all had relatively low levels of clinical disability (EDSS < 4). However, one previous study conducted in RRMS patients with EDSS scores lower than 1.5 still found the pattern of increased BOLD responses, interpreted as cortical recruitment, in these low-disability MS patients [139]. The non-significant results for the ROI analysis could instead be because of the ROI selection, as there were some BOLD group differences in the voxel-wise analysis that did not come out in the ROI analysis. An alternative explanation to this inconsistency is that different studies implement different techniques, and there could be an intrinsic property of specific implementation that is affecting the BOLD data. Additionally, although the most common BOLD finding in MS patients is an increased functional recruitment, there are many studies that suggest alternative patterns of BOLD-activation in MS patients, such as a relationship between BOLD activation and patient fatigue [141, 142]. This ambiguity in the BOLD MS literature is also likely partially due to the heterogeneity of MS pathology, as well as some variability in fMRI methods and data analysis techniques. In addition to the indirect nature of the BOLD signal, the inconsistency in BOLD finding in MS warrants further investigation into alternative fMRI measures, such as CBF.

CBF Results

Consistent with our BOLD ROI analysis and CBF voxel-wise analysis, the CBF ROI analysis revealed a significant effect of task, where the ME task had higher CBF psc than the MI task in the primary motor cortex and the primary somatosensory cortex.

Quantification of CBF psc also revealed a significant main effect of group, across both levels of task, in the primary motor cortex and the primary somatosensory cortex. The MS group had significantly higher CBF psc and significantly lower baseline CBF compared to the healthy control group, suggesting that the brains of these MS patients may be compensating for their pathology by increasing neural activity to complete a motor task. This is consistent with previously suggested mechanisms of functional plasticity that is thought to slow the progression of MS in RRMS patients. These findings are consistent with existing literature on normal appearing white matter (NAWM) in MS patients [2, 143, 144]; however, findings from CBF MS studies are also inconsistent, similar to the inconsistency of BOLD MS studies discussed previously. Some studies show increased baseline perfusion [1], others show decreased baseline perfusion [2], and others show regional perfusion differences [69] in MS. The explanation of these inconsistencies is likely similar to the reasoning behind similar inconsistencies in the BOLD literature. Additionally, the signal difference between the control and tag images in ASL data is as low as ~1% of the signal from the control image; this results in low tSNR and can affect accuracy of mapping blood flow. The intrinsically low tSNR of ASL CBF data may be another reason for inconsistency in previous studies.

In summary, the analysis of CBF data revealed group differences in motor task-induced hemodynamic processes that were not detected by looking at BOLD alone. This emphasizes the importance of looking at processes that underlie the BOLD response, rather than relying on

BOLD data alone. Review of the existing CBF literature demonstrates that additional exploration is required to validate our CBF conclusions and clarify the inconsistency of findings.

The inconsistency in findings in BOLD and CBF MS studies has significantly limited the ability of fMRI to enhance the understanding of MS pathophysiology. Additionally, the exact cause of this inconsistency is unknown, and is likely due to a multitude of factors, including patient-related factors, such as heterogeneity between MS patients, increased motion in patients, and/or reduced ability to perform motor tasks, and also methodological factors, such as the technology used to acquire the data, the analysis pipeline used to process the imaging data, the technique used to define ROIs, etc. These potentially confounding factors are further complicated by the fact that neither BOLD nor CBF are direct measures of neural activity, which may result in incorrect interpretations and erroneous conclusions. Although we also analyzed BOLD and CBF data, the aim of our study was to quantify $CMRO_2$, which is a more direct measure of neural activity, and also to investigate the relationship between $CMRO_2$ and CBF. Analysis of $CMRO_2$ in MS can help minimize the risk of incorrect interpretations of MS BOLD data and may help clarify the results of past and future fMRI studies in MS.

$CMRO_2$ Results

Previous research has shown that baseline global $CMRO_2$ is lower in MS patients compared to controls [3], however, no previous MS research exists on task-induced $\Delta CMRO_2$, which is a more direct measure of neural activity than BOLD because it reflects total energetic workload. The only significant effect found for $CMRO_2$ psc was an effect of task (ME>MI) in the primary motor cortex. No significant group differences were observed for any of the ROIs; however, the MS group had higher (non-significant) $CMRO_2$ psc in all three ROIs compared to

the controls. Although this difference was non-significant, it can be interpreted in the context of the previous BOLD psc and CBF psc findings; specifically, it can help explain the presence of higher CBF psc in the MS group but no difference in BOLD psc between the two groups. When interpreted together, the BOLD psc, CBF psc, and $CMRO_2$ psc findings indicate that low disability RRMS patients have altered cerebral physiology. Although no significant BOLD differences were found, this was not because of a lack of differences in neurovascular processes. Both CBF psc and $CMRO_2$ psc appear to be higher in the MS group, and when these two measures both increase, they cancel out each other's effect on BOLD. This finding further demonstrates why investigating the BOLD response alone, without looking at the other underlying physiological processes, can result in inaccurate conclusions. This may also partially explain the incongruity of fMRI results in MS patients, because the measures being studied, primarily BOLD, may not be sufficient on their own to provide accurate and consistent results.

The present findings can also contribute to the understanding of mitochondrial dysfunction in MS (discussed in Section 2.1.1), which has been suggested to largely mediate the neurodegenerative component of MS pathology that occurs in addition to the inflammatory/demyelinating processes [73]. Research suggests that mitochondrial dysfunction may be caused by the production of ROS and RNS, which are generated by macrophages and activated microglia in inflammatory lesions [73]. These reactive species can directly inhibit the electron transport chain, which interrupts the process of cellular respiration, therefore inhibiting the ability of mitochondria to properly function [73]. During an inflammatory demyelinating attack, this decreased functioning of mitochondria is likely associated with a decreased need for oxygen (i.e. decreased cerebral oxygen metabolism), because fewer mitochondria are able to use oxygen to produce ATP. However, after an inflammatory demyelinating attack, demyelinated

axons that are otherwise uninjured have been shown to contain increased levels of mitochondria, which is thought to be an adaptive phenomenon to compensate for local demyelination and neurodegeneration [73]. With increased levels of mitochondria comes an increase in the need for oxygen, which is essential to mitochondria's ability to produce ATP. Our results of increased CBF (significant) and $CMRO_2$ (non-significant) suggest that this compensatory mitochondrial response to demyelination is occurring in our MS group. This finding is consistent with the fact that our MS patients were all fairly low-disability and were all in periods of remission; therefore, these patients are likely successfully compensating for demyelination. Although further research is needed to confirm this compensatory theory, if true, this theory suggests that the progressive state of MS may be due to an inability to maintain the mitochondrial compensatory response to demyelination. Failure of this compensatory response would result in a lack of ATP production, therefore causing chronic neurodegeneration, which is suggested to be a key characteristic in progressive MS patients [73]. The lack of a compensatory mitochondria response would therefore be associated with lower $CMRO_2$ psc levels in these patients. Therefore, $CMRO_2$ may provide a useful measure of disease progression.

In general, previous MS studies that measured BOLD alone have similar conclusions about the presence of a compensatory process [42, 44, 50, 51, 60, 138, 140, 145]; however, $CMRO_2$ psc is a direct measure of mitochondria metabolism and therefore may provide a more accurate marker of this disease process. Although our findings suggest that $CMRO_2$ may provide a more accurate and consistent measure of neural activity compared to BOLD, further research is needed to validate these theories and determine if $CMRO_2$ does in fact follow the previously suggested pattern in MS patients with differing levels of disability and disease progression. Additionally, it is important to determine if the significant increase in CBF psc and the non-

significant increase in $CMRO_2$ that we see in MS patients compared to controls is associated with an impairment in neurovascular coupling (i.e. the flow-metabolism ratio), as this may alter our conclusions.

Flow-metabolism Results

This study is the first study to investigate the relationship between $CMRO_2$ and CBF (flow-metabolism ratio) in MS patients. Quantification of this ratio provides essential information about the processes underlying the BOLD response. Our two-way mixed effects ANOVA of the flow-metabolism ratio did not show any significant effects of group or task, and the reported values were in the range of what has been previously found for healthy controls [75-79]. Therefore, with respect to the aforementioned compensatory response of mitochondria, it appears that the vascular systems of these patients are able to successfully increase CBF in response to the increased oxygen demand from mitochondria. These findings suggest that the BOLD contrast can be interpreted that same way in low disability RRMS as it is in healthy controls; however, caution must be taken, as these findings are yet to be replicated. Additionally, BOLD is not quantitative nor is it a direct measure of neural activity; therefore, future studies should calculate $CMRO_2$, because it is more accurate than BOLD, and CBF, because it enables a more complete interpretation of the results.

To summarize, we observed consistent (i.e. across all ROIs) group differences in CBF psc and consistent group differences in $CMRO_2$; however, we did not observe consistent group differences for BOLD or the flow-metabolism ratio. Taken together, these findings point towards a compensatory response in these MS patients, which results in a need for more oxygen to complete a task, and therefore an increase in both CBF psc and $CMRO_2$. However, there are a

number of potentially confounding factors that may be affecting our findings; these limitations are discussed in Chapter 6.

5.2 Cerebrovascular reactivity

Cerebrovascular reactivity is the ability of the cerebral blood vessels to dilate in response to a stimulus or task. Healthy brain function is dependent on this ability of the blood vessels to regulate the delivery of oxygen and glucose to activated cortical regions. We quantified BOLD-CVR and CBF-CVR to determine if this ability is impaired in MS patients compared to healthy controls. For both measures of global CVR, there were no significant differences between the two groups, implying that CVR is not impaired in low-disability RRMS patients (**Figures 4.6, 4.7, and 4.8**).

This finding is consistent with a previous study that found no significant CVR differences between controls and MS patients in different disease activity levels, including both remission and relapse [70]. It should be noted that this study used Transcranial Doppler (TCD), not fMRI BOLD or ASL techniques. Another study, which used ASL, found a significant decrease in gray matter CVR in MS patients compared to healthy controls [1], therefore conflicting with the results of the present study. These conflicting results could be do to differences between the patient groups, such as the mean EDSS score, which in the previous study was slightly higher (2.9; range 1-6), and the previous study had a mixture of RRMS and SPMS patients. Additionally, the present student only had 11 controls and 12 patients, whereas the previous study had 19 participants in each group.

To further explore our results, we performed correlation analyses on BOLD-CVR and CBF-CVR with each other and with the following variables: age, disease duration, and EDSS.

BOLD-CVR and CBF-CVR were significantly correlated in both groups. This finding was expected because BOLD-CVR and CBF-CVR are two methods for measuring the same physiological process. Neither age nor disease duration were correlated with either measure of CVR. In the MS group, the EDSS score correlated with BOLD-CVR. This suggests that CVR may be abnormal in some MS patients, depending on the patient's clinical characteristics and disease severity. One could speculate that patients with higher EDSS scores need to compensate more, and therefore have increased CVR compared to controls and patients with lower EDSS scores. However, the fact that EDSS did not correlate with CBF-CVR complicates this finding, and implies that something else may be going on, and there may be additional physiological processes at play. Alternatively, the lack of correlation between EDSS and CBF-CVR may be a false negative, potentially due to the low tSNR of ASL, the small sample size and the low power of this study.

In summary, the dilatory ability of cerebral blood vessels was preserved in these MS patients; however, our correlation findings suggest that CVR might be impaired in MS patients with more severe levels of disability.

Chapter Six: Conclusions, Limitations, and Future Work

In conclusion, both primary research objectives were successfully addressed in this study. Our findings from objective 1 exemplify the benefits of quantitative fMRI. The combined analysis of BOLD, CBF, $CMRO_2$, and the flow-metabolism ratio revealed important characteristics about neurovascular processes in MS patients, including how these processes may be altered in MS, how these processes may confound the interpretation of the BOLD contrast in MS, and how these processes relate to the compensatory theory of MS and its complementary theory of MS progression. As an extension to objective 1, activation maps of ME and MI were compared within and between groups to determine if these two tasks show similar patterns of cortical activation. From these comparisons, we determined the applicability of motor imagery as an alternative task, independent of physical motor function, to access the motor network. Lastly, our findings from objective 2 indicate that CVR is normal in low disability RRMS patients, as it was not significantly different in the multiple sclerosis group compared to the healthy control group. It is important to note that our study included low disability RRMS patients only (EDSS $\leq$ 4); therefore, the applicability of our findings is limited to this specific sub-group of MS patients. Other limitations of this study are addressed below.

A potential limitation of this study, as is inherent to all statistical research experiments, is the risk of Type I and Type II errors. A number of factors in this study contribute to this risk, such as low sample size, insensitivity of methods, high variability of measures, low study power, heterogeneity of MS patients, etc. These limitations may be a primary reason for the disparity of fMRI results in MS studies. Unfortunately, this heterogeneity is innate to all MS research, and cannot be fully overcome. However, future research with a larger sample size plus the inclusion of relapsing remitting and progressive patients with a more extensive range of disability, would

enhance the ability to determine how patients differ, and how pathological differences correlate with behavioural differences. By helping to explain the heterogeneity that occurs in MS, this research would enhance the interpretation of other research findings on subgroups of MS patients. In addition to heterogeneity resulting from the MS disease itself, discrepancies in fMRI studies may be due to participants' individual differences in things such as medications, motion during the MRI, and the amount of caffeine intake before the MRI, which has been shown to effect fMRI measures [146]. The application of more stringent conditions and inclusion/exclusion criteria in future studies may help minimize these effects.

Another major limitation of this research is the amount of data that had to be excluded due to ghosting artifacts and low tSNR of ASL data. Future research should utilize more advanced technology, such as a head coil with more channels, and should also ensure all imaging sequence parameters are optimized to limit these issues. However, ultimately, the solution to these problems rests primarily on the development of more sensitive and accurate imaging techniques.

As neuroscience continues to advance in its ability to understand the brain, the available technology and methods must simultaneously advance to provide better physiological detail. This thesis presents the first study using advanced quantitative fMRI to study task-induced $CMRO_2$ psc and CBF:$CMRO_2$ in MS patients, and suggests that future MS research using these techniques may significantly contribute to explaining MS pathology and progression.

REFERENCES

1. Marshall, O., et al., *Impaired cerebrovascular reactivity in multiple sclerosis.* JAMA Neurol, 2014. **71**(10): p. 1275-81.
2. Steen, C., et al., *Cerebral white matter blood flow and energy metabolism in multiple sclerosis.* Multiple Sclerosis Journal, 2013. **19**(10): p. 1282-1289.
3. Ge, Y., et al., *Characterizing brain oxygen metabolism in patients with multiple sclerosis with T2-relaxation-under-spin-tagging MRI.* J Cereb Blood Flow Metab, 2012. **32**(3): p. 403-12.
4. Sharma, N. and J.C. Baron, *Does motor imagery share neural networks with executed movement: a multivariate fMRI analysis.* Front Hum Neurosci, 2013. **7**: p. 564.
5. MSSC., http://www.mssociety.ca/en/information. MS Society of Canada, 2009.
6. PA., C., *Diagnosis and management of multiple sclerosis.* Am Fam Physician, 2004. **70**(10): p. 1935-1944.
7. SD., C., *Multiple sclerosis: pathologic, clinical, and imaging updates.* Rev Neurol Dis 2006, 2006. **3**(1): p. 23-28.
8. Miller, A., *Diagnosis of multiple sclerosis.* Seminars in Neurology, 1998. **18**(3): p. 309-316.
9. Rosenblum D, S.M., *The natural history of multiple sclerosis and its diagnosis.* Physical Medicine & Rehabilitation Clinics of North America, 1998. **9**(3): p. 537-549.
10. Hankomaki, E., et al., *The progress of cognitive decline in newly diagnosed MS patients.* Acta Neurol Scand, 2014. **129**(3): p. 184-91.
11. Johansson, S., et al., *High concurrent presence of disability in multiple sclerosis. Associations with perceived health.* J Neurol, 2007. **254**(6): p. 767-73.
12. Rae-Grant, A.D., et al., *Sensory symptoms of multiple sclerosis: a hidden reservoir of morbidity.* Mult Scler, 1999. **5**(3): p. 179-83.
13. Hanken, K., P. Eling, and H. Hildebrandt, *Is there a cognitive signature for MS-related fatigue?* Mult Scler, 2015. **21**(4): p. 376-81.
14. Krupp, L.B., et al., *Fatigue in multiple sclerosis.* Arch Neurol, 1988. **45**(4): p. 435-7.
15. Freal, J.E., G.H. Kraft, and J.K. Coryell, *Symptomatic fatigue in multiple sclerosis.* Arch Phys Med Rehabil, 1984. **65**(3): p. 135-8.
16. Patten, S.B., et al., *Major depression in multiple sclerosis: a population-based perspective.* Neurology, 2003. **61**(11): p. 1524-7.
17. Korostil, M. and A. Feinstein, *Anxiety disorders and their clinical correlates in multiple sclerosis patients.* Mult Scler, 2007. **13**(1): p. 67-72.
18. Heremans, E., et al., *The relation between cognitive and motor dysfunction and motor imagery ability in patients with multiple sclerosis.* Mult Scler, 2012. **18**(9): p. 1303-9.
19. Benedict, R.H., et al., *Upper and lower extremity motor function and cognitive impairment in multiple sclerosis.* J Int Neuropsychol Soc, 2011. **17**(4): p. 643-53.
20. CWA., A., *The General Pathology of Multiple Sclerosis: Morphology and Chemical Aspects of the Lesions.* 1983: p. 203-240.
21. Weinshenker BG, R.G., Noseworthy JH, Carriere W, Baserville J, Erbers GC., *The Natural History of Multiple Sclerosis: A Geographically based Study.* Brain, 1991. **114**: p. 1057=1067.

22. Shi, J., L.C. Baxter, and S.M. Kuniyoshi, *Pathologic and imaging correlates of cognitive deficits in multiple sclerosis: changing the paradigm of diagnosis and prognosis.* Cogn Behav Neurol, 2014. **27**(1): p. 1-7.
23. Milo, R., *Effectiveness of multiple sclerosis treatment with current immunomodulatory drugs.* Expert Opin Pharmacother, 2015. **16**(5): p. 659-73.
24. Allegretta, M., et al., *T cells responsive to myelin basic protein in patients with multiple sclerosis.* Science, 1990. **247**(4943): p. 718-21.
25. Zhang, J., et al., *Increased frequency of interleukin 2-responsive T cells specific for myelin basic protein and proteolipid protein in peripheral blood and cerebrospinal fluid of patients with multiple sclerosis.* J Exp Med, 1994. **179**(3): p. 973-84.
26. Dendrou, C.A., L. Fugger, and M.A. Friese, *Immunopathology of multiple sclerosis.* Nat Rev Immunol, 2015. **15**(9): p. 545-58.
27. Hickey, W.F., B.L. Hsu, and H. Kimura, *T-lymphocyte entry into the central nervous system.* J Neurosci Res, 1991. **28**(2): p. 254-60.
28. Friese, M.A., B. Schattling, and L. Fugger, *Mechanisms of neurodegeneration and axonal dysfunction in multiple sclerosis.*
29. O'Gorman, C., R. Lucas, and B. Taylor, *Environmental risk factors for multiple sclerosis: a review with a focus on molecular mechanisms.* Int J Mol Sci, 2012. **13**(9): p. 11718-52.
30. Holick, M.F., *Sunlight and vitamin D for bone health and prevention of autoimmune diseases, cancers, and cardiovascular disease.* Am J Clin Nutr, 2004. **80**(6 Suppl): p. 1678s-88s.
31. Sloka, S., et al., *A quantitative analysis of suspected environmental causes of MS.* Can J Neurol Sci, 2011. **38**(1): p. 98-105.
32. Haahr, S., et al., *A role of late Epstein-Barr virus infection in multiple sclerosis.* Acta Neurol Scand, 2004. **109**(4): p. 270-5.
33. Nortvedt, M.W., et al., *Prevalence of bladder, bowel and sexual problems among multiple sclerosis patients two to five years after diagnosis.* Mult Scler, 2007. **13**(1): p. 106-12.
34. Marrie, R., et al., *High frequency of adverse health behaviors in multiple sclerosis.* Mult Scler, 2009. **15**(1): p. 105-13.
35. Beecham, A.H., et al., *Analysis of immune-related loci identifies 48 new susceptibility variants for multiple sclerosis.* Nat Genet, 2013. **45**(11): p. 1353-60.
36. McDonald WI, C.A., Edan G, Goodkin D, Hartung HP, Lublin FD, McFarland HF, Paty DW, Polman CH, Reingold SC, Sandberg-Wollheim M, Sibley W, Thompson A, S vdN, Weinshenker BY, Wolinsky JS., *Recommended diagnostic criteria for multiple sclerosis: Guidelines from the International Panel on the diagnosis of multiple sclerosis.* Ann Neurol, 2001. **50**(1): p. 121-127.
37. Miller DH, W.B., Filippi M, Banwell BL, Cohen JA, Freedman MS, Galetta SL, Hutchinson M, Johnson RT, Kappos L, Kira J, Lublin FD, McFarland HF, Montalban X, Panitch H, Richert JR, Reingold SC, Polman CH., *Differential diagnosis of suspected multiple sclerosis: a consensus approach.* Mult Scler, 2008. **14**(9): p. 1157-1174.
38. Polman CH, W.J., Reingold SC., *Multiple sclerosis diagnostic criteria: three years later.* Mult Scler, 2005. **11**(1): p. 5-12.
39. Polman CH, R.S., Edan G, Filippi M, Hartung HP, Kappos L, Lublin FD, Metz LM, McFarland HF, O'Connor PW, Sandberg-Wollheim M, Thompson AJ, Weinshenker BG,

Wolinsky JS., *Diagnostic criteria for multiple sclerosis: 2005 revisions to the "McDonald Criteria".* Ann Neurol, 2005. **58**(6): p. 840-846.
40. Kurtzke, J.F., *Rating neurologic impairment in multiple sclerosis an expanded disability status scale (EDSS).* Neurology, 1983. **33**(11): p. 1444-1444.
41. Hurwitz, B.J., *The diagnosis of multiple sclerosis and the clinical subtypes.* Ann Indian Acad Neurol, 2009. **12**(4): p. 226-30.
42. Lee, M., et al., *The motor cortex shows adaptive functional changes to brain injury from multiple sclerosis.* Ann Neurol, 2000. **47**(5): p. 606-13.
43. Reddy, H., et al., *Evidence for adaptive functional changes in the cerebral cortex with axonal injury from multiple sclerosis.* Brain, 2000. **123**(11): p. 2314-2320.
44. Reddy, H., et al., *Functional brain reorganization for hand movement in patients with multiple sclerosis: defining distinct effects of injury and disability.* Brain, 2002. **125**(Pt 12): p. 2646-57.
45. Bo, L., et al., *Grey matter pathology in multiple sclerosis.* Acta Neurol Scand Suppl, 2006. **183**: p. 48-50.
46. Bushberg, J.T. and J.M. Boone, *The essential physics of medical imaging*. 2011: Lippincott Williams & Wilkins.
47. Ogawa, S., et al., *Intrinsic signal changes accompanying sensory stimulation: functional brain mapping with magnetic resonance imaging.* Proc Natl Acad Sci U S A, 1992. **89**(13): p. 5951-5.
48. Williams, D.S., et al., *Magnetic resonance imaging of perfusion using spin inversion of arterial water.* Proc Natl Acad Sci U S A, 1992. **89**(1): p. 212-6.
49. Detre, J.A., et al., *Perfusion imaging.* Magn Reson Med, 1992. **23**(1): p. 37-45.
50. Bakshi, R., et al., *MRI in multiple sclerosis: current status and future prospects.* Lancet Neurol, 2008. **7**(7): p. 615-25.
51. Pelletier, J., et al., *Plasticity in MS: from Functional Imaging to Rehabilitation.* Int MS J, 2009. **16**(1): p. 26-31.
52. Kwong, K.K., et al., *Dynamic magnetic resonance imaging of human brain activity during primary sensory stimulation.* Proc Natl Acad Sci U S A, 1992. **89**(12): p. 5675-9.
53. Kwong, K., et al., *Functional MR imaging of primary visual and motor cortex.* JMRI, 1992. **2**(P): p. 76.
54. Vafaee, M.S., et al., *Oxygen consumption and blood flow coupling in human motor cortex during intense finger tapping: implication for a role of lactate.* J Cereb Blood Flow Metab, 2012. **32**(10): p. 1859-68.
55. Chiarelli, P.A., et al., *Flow-metabolism coupling in human visual, motor, and supplementary motor areas assessed by magnetic resonance imaging.* Magn Reson Med, 2007. **57**(3): p. 538-47.
56. Buxton, R.B., *Interpreting oxygenation-based neuroimaging signals: the importance and the challenge of understanding brain oxygen metabolism.* Front Neuroenergetics, 2010. **2**: p. 8.
57. Arthurs, O.J. and S. Boniface, *How well do we understand the neural origins of the fMRI BOLD signal?* Trends Neurosci, 2002. **25**(1): p. 27-31.
58. Specogna, I., et al., *Functional MRI during the execution of a motor task in patients with multiple sclerosis and fatigue.* Radiol Med, 2012. **117**(8): p. 1398-407.

59. Audoin, B., et al., *Compensatory cortical activation observed by fMRI during a cognitive task at the earliest stage of multiple sclerosis.* Human brain mapping, 2003. **20**(2): p. 51-58.
60. Rocca, M.A. and M. Filippi, *Functional MRI in multiple sclerosis.* J Neuroimaging, 2007. **17 Suppl 1**: p. 36s-41s.
61. Pantano, P., et al., *A longitudinal fMRI study on motor activity in patients with multiple sclerosis.* Brain, 2005. **128**(Pt 9): p. 2146-53.
62. Filippi, M., et al., *A functional MRI study of cortical activations associated with object manipulation in patients with MS.* Neuroimage, 2004. **21**(3): p. 1147-54.
63. Loitfelder, M., et al., *Brain activity changes in cognitive networks in relapsing-remitting multiple sclerosis - insights from a longitudinal FMRI study.* PLoS One, 2014. **9**(4): p. e93715.
64. Tomassini, V., et al., *Neuroplasticity and functional recovery in multiple sclerosis.* Nat Rev Neurol, 2012. **8**(11): p. 635-46.
65. Mark, C.I., E.L. Mazerolle, and J.J. Chen, *Metabolic and vascular origins of the BOLD effect: Implications for imaging pathology and resting-state brain function.* J Magn Reson Imaging, 2015.
66. Blockley, N.P., et al., *A review of calibrated blood oxygenation level-dependent (BOLD) methods for the measurement of task-induced changes in brain oxygen metabolism.* NMR Biomed, 2013. **26**(8): p. 987-1003.
67. Rashid, W., et al., *Abnormalities of cerebral perfusion in multiple sclerosis.* J Neurol Neurosurg Psychiatry, 2004. **75**(9): p. 1288-93.
68. Bester, M., et al., *Increased perfusion in normal appearing white matter in high inflammatory multiple sclerosis patients.* PLoS One, 2015. **10**(3): p. e0119356.
69. Li, L., et al., *Perfusion and Diffusion Abnormalities of Multiple Sclerosis Lesions and Relevance of Classified Lesions to Disease Status.* J Neurol Neurophysiol, 2014. **2014**(Suppl 12): p. 12.
70. Uzuner, N., S. Ozkan, and N. Cinar, *Cerebrovascular reactivity in multiple sclerosis patients.* Mult Scler, 2007. **13**(6): p. 737-41.
71. Su, K.G., et al., *Axonal degeneration in multiple sclerosis: the mitochondrial hypothesis.* Curr Neurol Neurosci Rep, 2009. **9**(5): p. 411-7.
72. Haider, L., et al., *Oxidative damage in multiple sclerosis lesions.* Brain, 2011. **134**(Pt 7): p. 1914-24.
73. Witte, M.E., et al., *Mitochondrial dysfunction contributes to neurodegeneration in multiple sclerosis.* Trends Mol Med, 2014. **20**(3): p. 179-87.
74. Fan, A.P., et al., *Quantitative oxygen extraction fraction from 7-Tesla MRI phase: reproducibility and application in multiple sclerosis.* J Cereb Blood Flow Metab, 2015. **35**(1): p. 131-9.
75. Pike, G.B., *Quantitative functional MRI: concepts, issues and future challenges.* Neuroimage, 2012. **62**(2): p. 1234-40.
76. Fox, P.T. and M.E. Raichle, *Focal physiological uncoupling of cerebral blood flow and oxidative metabolism during somatosensory stimulation in human subjects.* Proc Natl Acad Sci U S A, 1986. **83**(4): p. 1140-4.
77. Hoge, R.D., et al., *Linear coupling between cerebral blood flow and oxygen consumption in activated human cortex.* Proc Natl Acad Sci U S A, 1999. **96**(16): p. 9403-8.

78. Kastrup, A., et al., *Changes of cerebral blood flow, oxygenation, and oxidative metabolism during graded motor activation.* Neuroimage, 2002. **15**(1): p. 74-82.
79. Donahue, M.J., et al., *Cerebral blood flow, blood volume, and oxygen metabolism dynamics in human visual and motor cortex as measured by whole-brain multi-modal magnetic resonance imaging.* J Cereb Blood Flow Metab, 2009. **29**(11): p. 1856-66.
80. Warnking JM, P.G., *Bandwidth-modulated adiabatic RF pulses for uniform selective saturation and inversion.* Magnetic resonance in medicine: official journal of the Society of Magnetic Resonance in Medicine / Society of Magnetic Resonance in Medicine 2004;52(5):1190-1199., 2004. **52**(5): p. 1190-1199.
81. Chen, J.J. and G.B. Pike, *MRI measurement of the BOLD-specific flow-volume relationship during hypercapnia and hypocapnia in humans.* Neuroimage, 2010. **53**(2): p. 383-91.
82. Chen, J.J. and G.B. Pike, *Global cerebral oxidative metabolism during hypercapnia and hypocapnia in humans: implications for BOLD fMRI.* J Cereb Blood Flow Metab, 2010. **30**(6): p. 1094-9.
83. Mark, C.I., J.A. Fisher, and G.B. Pike, *Improved fMRI calibration: Precisely controlled hyperoxic versus hypercapnic stimuli.* Neuroimage, 2011. **54**(2): p. 1102-1111.
84. Davis, T.L., et al., *Calibrated functional MRI: mapping the dynamics of oxidative metabolism.* Proc Natl Acad Sci U S A, 1998. **95**(4): p. 1834-9.
85. Hoge, R.D., et al., *Investigation of BOLD signal dependence on cerebral blood flow and oxygen consumption: the deoxyhemoglobin dilution model.* Magn Reson Med, 1999. **42**(5): p. 849-63.
86. Weinshenker, B.G., et al., *The natural history of multiple sclerosis: a geographically based study. I. Clinical course and disability.* Brain, 1989. **112 (Pt 1)**: p. 133-46.
87. Kurtzke, J.F., *Rating neurologic impairment in multiple sclerosis: an expanded disability status scale (EDSS).* Neurology, 1983. **33**(11): p. 1444-52.
88. S.F. Storti, I.B.G., F. Pizzini, S. Montemezzi, R. Manganotti, G. Menegaz, *Sensitivity of BOLD and perfusion contrasts derived from dual-echo ASL in localising active an imaginary movements*, in *ISMRM*. 2015, ISMRM: Toronto, Canada.
89. Sharma, N., et al., *Mapping the involvement of BA 4a and 4p during Motor Imagery.* Neuroimage, 2008. **41**(1): p. 92-9.
90. Peirce, J.W., *PsychoPy--Psychophysics software in Python.* J Neurosci Methods, 2007. **162**(1-2): p. 8-13.
91. Cutter, G.R., et al., *Development of a multiple sclerosis functional composite as a clinical trial outcome measure.* Brain, 1999. **122**(5): p. 871-882.
92. Rudick, R., et al., *Clinical outcomes assessment in multiple sclerosis.* Annals of neurology, 1996. **40**(3): p. 469-479.
93. Smith, A., *Symbol digit modalities test: Manual*. 2002: Western Psychological Corporation.
94. Fisk, J.D., et al., *Measuring the functional impact of fatigue: initial validation of the fatigue impact scale.* Clin Infect Dis, 1994. **18 Suppl 1**: p. S79-83.
95. Veit, C.T. and J.E. Ware, Jr., *The structure of psychological distress and well-being in general populations.* J Consult Clin Psychol, 1983. **51**(5): p. 730-42.
96. Smith, S.M., et al., *Advances in functional and structural MR image analysis and implementation as FSL.* Neuroimage, 2004. **23 Suppl 1**: p. S208-19.

97. Ashburner, J., et al., *SPM8 manual.* Functional Imaging Laboratory, Institute of Neurology, 2012.
98. Bulte, D.P., et al., *Quantitative measurement of cerebral physiology using respiratory-calibrated MRI.* Neuroimage, 2012. **60**(1): p. 582-91.
99. Schmithorst, V.J., et al., *Evidence that neurovascular coupling underlying the BOLD effect increases with age during childhood.* Hum Brain Mapp, 2015. **36**(1): p. 1-15.
100. Smith, S.M., et al., *Variability in fMRI: a re-examination of inter-session differences.* Hum Brain Mapp, 2005. **24**(3): p. 248-57.
101. Wang, Z., *Improving cerebral blood flow quantification for arterial spin labeled perfusion MRI by removing residual motion artifacts and global signal fluctuations.* Magnetic resonance imaging, 2012. **30**(10): p. 1409-1415.
102. Wang, Z., et al., *Empirical optimization of ASL data analysis using an ASL data processing toolbox: ASLtbx.* Magnetic resonance imaging, 2008. **26**(2): p. 261-269.
103. Smith, S.M., *Fast robust automated brain extraction.* Human brain mapping, 2002. **17**(3): p. 143-155.
104. Chappell, M.A., et al., *Variational Bayesian inference for a nonlinear forward model.* Trans. Sig. Proc., 2009. **57**(1): p. 223-236.
105. Jenkinson, M., et al., *Improved optimization for the robust and accurate linear registration and motion correction of brain images.* Neuroimage, 2002. **17**(2): p. 825-841.
106. Jenkinson, M. and S. Smith, *A global optimisation method for robust affine registration of brain images.* Medical image analysis, 2001. **5**(2): p. 143-156.
107. Greve, D.N. and B. Fischl, *Accurate and robust brain image alignment using boundary-based registration.* Neuroimage, 2009. **48**(1): p. 63-72.
108. Lancaster, J.L., et al., *Automated Talairach atlas labels for functional brain mapping.* Human brain mapping, 2000. **10**(3): p. 120-131.
109. Maldjian, J.A., et al., *An automated method for neuroanatomic and cytoarchitectonic atlas-based interrogation of fMRI data sets.* Neuroimage, 2003. **19**(3): p. 1233-1239.
110. Worsley, K., *Statistical analysis of activation images.* Functional MRI: An introduction to methods, 2001. **14**: p. 251-70.
111. Hare, H.V., et al., *Comparison of CO2 in air versus carbogen for the measurement of cerebrovascular reactivity with magnetic resonance imaging.* Journal of Cerebral Blood Flow & Metabolism, 2013. **33**(11): p. 1799-1805.
112. Toga, A.W., et al., *Towards multimodal atlases of the human brain.* Nature Reviews Neuroscience, 2006. **7**(12): p. 952-966.
113. Eickhoff, S.B., et al., *Assignment of functional activations to probabilistic cytoarchitectonic areas revisited.* Neuroimage, 2007. **36**(3): p. 511-521.
114. Eickhoff, S.B., et al., *A new SPM toolbox for combining probabilistic cytoarchitectonic maps and functional imaging data.* Neuroimage, 2005. **25**(4): p. 1325-1335.
115. Zhang, Y., M. Brady, and S. Smith, *Segmentation of brain MR images through a hidden Markov random field model and the expectation-maximization algorithm.* Medical Imaging, IEEE Transactions on, 2001. **20**(1): p. 45-57.
116. Boxerman, J.L., et al., *MR contrast due to intravascular magnetic susceptibility perturbations.* Magn Reson Med, 1995. **34**(4): p. 555-66.

117. Mark CI, F.J., Pike GB., *Improved fMRI calibration: Precisely controlled hyperoxic versus hypercapnic stimuli.* NeuroImage, 2011. **54**(2): p. 1102-1111.
118. Grubb, R.L., Jr., et al., *The effects of changes in PaCO2 on cerebral blood volume, blood flow, and vascular mean transit time.* Stroke, 1974. **5**(5): p. 630-9.
119. Chen, J.J. and G.B. Pike, *BOLD-specific cerebral blood volume and blood flow changes during neuronal activation in humans.* NMR Biomed, 2009. **22**(10): p. 1054-62.
120. Poulin, M.J., P.J. Liang, and P.A. Robbins, *Dynamics of the cerebral blood flow response to step changes in end-tidal PCO2 and PO2 in humans.* J Appl Physiol (1985), 1996. **81**(3): p. 1084-95.
121. Mark, C.I. and G.B. Pike, *Indication of BOLD-specific venous flow-volume changes from precisely controlled hyperoxic vs. hypercapnic calibration.* J Cereb Blood Flow Metab, 2012. **32**(4): p. 709-19.
122. Beckmann, C.F., M. Jenkinson, and S.M. Smith, *General multilevel linear modeling for group analysis in FMRI.* Neuroimage, 2003. **20**(2): p. 1052-1063.
123. Woolrich, M.W., et al., *Multilevel linear modelling for FMRI group analysis using Bayesian inference.* Neuroimage, 2004. **21**(4): p. 1732-1747.
124. Woolrich, M., *Robust group analysis using outlier inference.* Neuroimage, 2008. **41**(2): p. 286-301.
125. van der Zwaag, W., et al., *Minimization of Nyquist ghosting for echo-planar imaging at ultra-high fields based on a "negative readout gradient" strategy.* J Magn Reson Imaging, 2009. **30**(5): p. 1171-8.
126. Schmitt, F., M.K. Stehling, and R. Turner, *Echo-planar imaging: theory, technique and application*. 2012: Springer Science & Business Media.
127. Pruessmann, K.P., et al., *SENSE: sensitivity encoding for fast MRI.* Magn Reson Med, 1999. **42**(5): p. 952-62.
128. King, K.F. *ASSET–Parallel Imaging on the GE Scanner*. in *2nd international workshop on parallel MRI; October*. 2004.
129. Creem-Regehr, S.H., *Sensory-motor and cognitive functions of the human posterior parietal cortex involved in manual actions.* Neurobiol Learn Mem, 2009. **91**(2): p. 166-71.
130. Johnson-Frey, S.H., R. Newman-Norlund, and S.T. Grafton, *A distributed left hemisphere network active during planning of everyday tool use skills.* Cereb Cortex, 2005. **15**(6): p. 681-95.
131. Rushworth, M.F., et al., *The left parietal and premotor cortices: motor attention and selection.* Neuroimage, 2003. **20 Suppl 1**: p. S89-100.
132. Grefkes, C., et al., *Dynamic intra- and interhemispheric interactions during unilateral and bilateral hand movements assessed with fMRI and DCM.* Neuroimage, 2008. **41**(4): p. 1382-94.
133. Shibasaki, H., *Cortical activities associated with voluntary movements and involuntary movements.* Clin Neurophysiol, 2012. **123**(2): p. 229-43.
134. Lacourse, M.G., et al., *Brain activation during execution and motor imagery of novel and skilled sequential hand movements.* Neuroimage, 2005. **27**(3): p. 505-19.
135. Hanakawa, T., et al., *Functional properties of brain areas associated with motor execution and imagery.* J Neurophysiol, 2003. **89**(2): p. 989-1002.

136. Sharma, N., V.M. Pomeroy, and J.C. Baron, *Motor imagery: a backdoor to the motor system after stroke?* Stroke, 2006. **37**(7): p. 1941-52.
137. Liu, H., L. Song, and T. Zhang, *Changes in brain activation in stroke patients after mental practice and physical exercise: a functional MRI study.* Neural Regen Res, 2014. **9**(15): p. 1474-84.
138. Fox, R.J., et al., *Advanced MRI in multiple sclerosis: current status and future challenges.* Neurol Clin, 2011. **29**(2): p. 357-80.
139. Colorado, R.A., et al., *Multi-task functional MRI in multiple sclerosis patients without clinical disability.* Neuroimage, 2012. **59**(1): p. 573-81.
140. Filippi, M. and M.A. Rocca, *Cortical reorganisation in patients with MS.* J Neurol Neurosurg Psychiatry, 2004. **75**(8): p. 1087-9.
141. White, A.T., et al., *Brain activation in multiple sclerosis: a BOLD fMRI study of the effects of fatiguing hand exercise.* Mult Scler, 2009. **15**(5): p. 580-6.
142. Filippi, M., et al., *Functional magnetic resonance imaging correlates of fatigue in multiple sclerosis.* Neuroimage, 2002. **15**(3): p. 559-67.
143. Ota, M., et al., *Abnormalities of cerebral blood flow in multiple sclerosis: a pseudocontinuous arterial spin labeling MRI study.* Magn Reson Imaging, 2013. **31**(6): p. 990-5.
144. Law, M., et al., *Microvascular abnormality in relapsing-remitting multiple sclerosis: perfusion MR imaging findings in normal-appearing white matter.* Radiology, 2004. **231**(3): p. 645-52.
145. Reddy, H., et al., *Evidence for adaptive functional changes in the cerebral cortex with axonal injury from multiple sclerosis.* Brain, 2000. **123 (Pt 11)**: p. 2314-20.
146. Xu, F., et al., *Does acute caffeine ingestion alter brain metabolism in young adults?* Neuroimage, 2015. **110**: p. 39-47.